

# Nonparametric Bellman Mappings for Value Iteration in Distributed Reinforcement Learning

Yuki Akiyama and Konstantinos Slavakis\*

**Abstract**—This paper introduces novel Bellman mappings (B-Maps) for value iteration (VI) in distributed reinforcement learning (DRL), where multiple agents operate over a network without a centralized fusion node. Each agent constructs its own nonparametric B-Map for VI while communicating only with direct neighbors to achieve consensus. These B-Maps operate on Q-functions represented in a reproducing kernel Hilbert space, enabling a nonparametric formulation that allows for flexible, agent-specific basis function design. Unlike existing DRL methods that restrict information exchange to Q-function estimates, the proposed framework also enables agents to share basis information in the form of covariance matrices, capturing additional structural details. A theoretical analysis establishes linear convergence rates for both Q-function and covariance-matrix estimates toward their consensus values. The optimal learning rates for consensus-based updates are dictated by the ratio of the smallest positive eigenvalue to the largest one of the network’s Laplacian matrix. Furthermore, each nodal Q-function estimate is shown to lie very close to the fixed point of a centralized nonparametric B-Map, effectively allowing the proposed DRL design to approximate the performance of a centralized fusion center. Numerical experiments on two well-known control problems demonstrate the superior performance of the proposed nonparametric B-Maps compared to prior methods. Notably, the results reveal a counter-intuitive finding: although the proposed approach involves greater information exchange—specifically through the sharing of covariance matrices—it achieves the desired performance with lower cumulative communication cost than existing DRL schemes, highlighting the crucial role of basis information in accelerating the learning process.

**Index Terms**—Reinforcement learning, distributed, Bellman mapping, nonparametric.

## I. INTRODUCTION

Reinforcement learning (RL) has been a widely studied field for many years [1], [2], [3]. In RL, an agent interacts with and controls a system by making sequential decisions or actions based on feedback from the surrounding environment. This feedback is typically provided in the form of an *one-step loss*  $g(\cdot)$  or, equivalently, a reward defined as  $-g(\cdot)$  [2], [3]. The agent uses this feedback to learn an *optimal policy*  $\mu_*(\cdot)$ , a function or strategy that prescribes actions, based on the system’s state, to minimize the *long-term loss/penalty*—also known as the Q-function. This Q-function represents the total penalty the agent would incur if all future decisions were made according to  $\mu_*(\cdot)$ . The Bellman mapping (B-Map) is a fundamental tool for computing Q-functions, with its fixed points playing a crucial role in determining optimal policies [2]. Over the years, various B-Map formulations and algorithmic approaches have been developed to model and

compute Q-functions. These include classical Q-learning [3], [2] as well as methods that employ function approximation [4], [5], [6], [7], [8], [9], [10], [11], [12].

This work builds on the framework of distributed reinforcement learning (DRL) and, more broadly, distributed learning [13], where multiple agents are deployed across a network or graph, with each agent assigned to a network node. Agents interact with a shared environment but are not required to exchange any state-action information. Each agent independently computes its Q-function estimates and shares them only with its neighboring agents—without relying on a central coordinator such as a “master node” or “fusion center.” Through this local exchange, agents collectively reach a consensus on a network-wide Q-function, enabling the identification of optimal policies [14], [15], [16], [17], [18].

Classical Q-learning has been extended into DRL, where, as is often the case in Q-learning, the state space is considered discrete rather than continuous, and Q-functions are represented in a tabular form [19], [14], [15]. Similarly, standard B-Maps have also been adapted for DRL in [14], [15], but the state space remains discrete, and the network or graph topology depends on the specific state space.

To overcome the limitations of tabular Q-functions and discrete state spaces, function approximation models for Q-functions have been explored, particularly in deep-learning-based DRL [20], [21], where a “master node” is assumed to exist within the network. DRL with function approximation has also been developed for fully distributed settings, eliminating the need for a master node, fusion center, or even partial state-information sharing among agents [17], [16], [18], [14], [15], [20], [22]. DRL significantly overlaps with multi-agent reinforcement learning (MARL), where the objective remains to compute a network-wide Q-function using information gathered across the network. However, in MARL, it is often assumed that agents share (partial) state information [19], [23], [24], [22], [21]. Notably, the MARL approach in [22] can operate in environments where state-space information is either shared or not shared. Additionally, distributed learning methods, such as [25], can accommodate general function-approximation models for Q-functions, including neural networks, and can be applied to address general and fully distributed DRL tasks.

This paper builds upon the benefits of the recently introduced nonparametric B-Maps [12] and extends them to DRL. Specifically, the B-Maps in this study operate on Q-functions within a reproducing kernel Hilbert space (RKHS) [26], [27], leveraging both the function-approximation capabilities of RKHS and the reproducing property of its inner product. This contrasts with standard B-Maps, where Q-functions are treated as elements of a Banach space (no inner-product structure) [2],

\*Y. Akiyama and K. Slavakis are with the Institute of Science Tokyo, Department of Information and Communications Engineering, 4259-G2-4 Nagatsuta-Cho, Midori-Ku, Yokohama, Kanagawa, 226-8502 Japan. Email: slavakis@ict.eng.isct.ac.jp.

[4]. By choosing an RKHS as the function-approximation space for Q-functions, the proposed approach is rendered nonparametric [28], eliminating the need for statistical priors and assumptions on the data while minimizing user-induced modeling bias. However, a key trade-off of this distribution-free approach is that the number of free parameters required to represent Q-function estimates grows with the amount of data. To address this challenge, a dimensionality-reduction strategy based on random Fourier features (RFF) [29] is introduced, mitigating the effects of the “curse of dimensionality.”

Each agent in this study constructs its own B-Map, specifically tailored to implement the classical value-iteration (VI) strategy in RL [2]. The proposed B-Maps are built using reproducing-kernel functions, parameterized by the data available to each agent  $n$ , where  $n \in \{1, \dots, N\}$ , along with agent-specific basis functions  $\Psi^{(n)}$ , which generally vary across agents. A key advantage inherited from [12] is the flexibility in designing  $\Psi^{(n)}$ . In fact, [12] demonstrates that carefully chosen  $\Psi^{(n)}$  can lead to popular B-Maps. Furthermore, the same work provides a variational framework for systematically designing  $\Psi^{(n)}$ , enabling principled and effective basis design.

This paper offers the following novel contributions to DRL.

### Contributions.

- (1) **(Novel B-Maps for DRL)** The benefits of the nonparametric B-Maps of [12] are extended to DRL. Each agent  $n$  has the flexibility to design its own basis functions  $\Psi^{(n)}$ , enabling the construction of *agent-specific* B-Maps.
- (2) **(Exchange of covariance-matrix data)** Unlike prior methods [17], [16], [18], [14], [15], [20], [22], [23], [24], where agents share only copies of their Q-function estimates, the proposed framework allows agents to also exchange information about their bases through covariance matrices.
- (3) **(Performance analysis and convergence)** The framework ensures linear convergence of both the nodal Q-function and covariance-matrix estimates toward their consensus values. The optimal learning rates for the iterative updates are governed by the ratio of the smallest positive eigenvalue to the largest one of the graph Laplacian matrix. Moreover, a tunable bound is established on the deviation of each nodal Q-function estimate from the fixed point of a centralized nonparametric B-Map. By adjusting a design parameter, this bound can be made arbitrarily small, suggesting that the proposed DRL design closely approximates the behavior of a centralized fusion center.

Numerical tests reveal a surprising, counter-intuitive result: although the proposed method involves exchanging *more* information among agents than prior approaches—specifically, through the sharing of covariance data matrices (Contribution (2))—it achieves desired performance with *less* communication cost than prior-art schemes. This underscores the significance of basis information, as its exchange accelerates the learning process.

## II. DISTRIBUTED REINFORCEMENT LEARNING

### A. Preliminaries and notation

A number  $N$  of agents are considered, distributed over a connected [30] network/graph  $\mathcal{G} := (\mathcal{N}, \mathcal{E})$ , with nodes  $\mathcal{N} := \{1, \dots, N\}$  and edges  $\mathcal{E}$ . The neighborhood of node  $n \in \mathcal{N}$  is defined as  $\mathcal{N}_n := \{n' \in \mathcal{N} \mid \{n, n'\} \in \mathcal{E}\}$ .

All agents share a common surrounding environment  $\{\mathcal{S}, \mathcal{A}, g(\cdot)\}$ , where  $\mathcal{S}$  and  $\mathcal{A}$  stand for the state and action space, respectively, and  $g(\cdot)$  is the one-step loss function. The state-action space is defined as  $\mathcal{Z} := \mathcal{S} \times \mathcal{A} := \{z := (s, a) \mid s \in \mathcal{S}, a \in \mathcal{A}\}$ . A state and action at agent  $n$  will be denoted henceforth by  $s_i^{(n)} \in \mathcal{S}$  and  $a_i^{(n)} \in \mathcal{A}$ , respectively, where  $i$  serves as a non-negative integer ordering index, as in sequences  $(s_i^{(n)})_{i=0}^\infty$  and  $(a_i^{(n)})_{i=0}^\infty$ , for example.

Agent  $n$  uses its current state  $s_i^{(n)}$  and policy  $\mu^{(n)}: \mathcal{S} \rightarrow \mathcal{A}$  to take action  $a_i^{(n)} := \mu^{(n)}(s_i^{(n)})$ . Then, the environment provides feedback  $g_i^{(n)} := g(z_i^{(n)})$  to the agent, with  $z_i^{(n)} := (s_i^{(n)}, a_i^{(n)})$ , via the one-step loss  $g: \mathcal{Z} \rightarrow \mathbb{R}$ , for the agent to transition to the new state  $s_{i+1}^{(n)} := s_i^{(n)'}$ . This transition obeys a conditional probability density function (PDF)  $p(s_{i+1}^{(n)} \mid s_i^{(n)}, a_i^{(n)})$ . This manuscript assumes that *none* of the agents has *any* information on this conditional PDF.

In RL with function approximation, Q-functions are considered to be elements of some functional space  $\mathcal{H}$ . The classical B-Map  $T_\diamond: \mathcal{H} \rightarrow \mathcal{H}$  describes a “total loss,” comprising the one-step loss and the expected “minimum” long-term loss (Q-function):  $\forall Q^{(n)} \in \mathcal{H}, \forall z = (s, a) \in \mathcal{Z}$ ,

$$(T_\diamond Q^{(n)})(z) := g(z) + \alpha \mathbb{E}_{s' \mid z} \{ \inf_{a' \in \mathcal{A}} Q^{(n)}(s', a') \}, \quad (1)$$

where  $Q^{(n)}$  and  $T_\diamond Q^{(n)}$  are functions defined on  $\mathcal{Z}$ ,  $\alpha \in \mathbb{R}_{++}$  is the discount factor, and  $\mathbb{E}_{s' \mid z} \{\cdot\}$  stands for conditional expectation, with  $s'$  standing for the potential next state after the agent takes action  $a$  at state  $s$ . A recursive application of (1) defines the classical *value-iteration* (VI) strategy of RL [2]. For any  $Q^{(n)} \in \mathcal{H}$  available to agent  $n$  in state  $s \in \mathcal{S}$ , action  $a$  can be taken in the following classical way [1], [2]:

$$a \in \arg \inf_{a' \in \mathcal{A}} Q^{(n)}(s, a'). \quad (2)$$

This operation defines also a set-valued policy  $\mu^{(n)}(s; Q^{(n)}) := \arg \inf_{a' \in \mathcal{A}} Q^{(n)}(s, a')$ , parameterized by  $Q^{(n)}$ . It is also well-known that a “desirable” total loss  $Q_\diamond^{(n)}$  is a fixed-point of  $T_\diamond$ , that is,  $Q_\diamond^{(n)} \in \text{Fix } T_\diamond := \{Q \in \mathcal{H} \mid T_\diamond Q = Q\}$  [2]. If  $\mathbb{E}_{s' \mid z} \{\cdot\}$  is available, the computation of  $T_\diamond$  and any of its fixed points can be performed at every agent  $n$  independently from all other agents.

Following the nonparametric framework of [12], Q-functions will be henceforth considered to be elements of a reproducing kernel Hilbert space (RKHS)  $\mathcal{H}$  [26], [27], common to all agents. The functional space  $\mathcal{H}$  is potentially infinite dimensional [26], [27], equipped with an inner product  $\langle \cdot \mid \cdot \rangle_{\mathcal{H}}$ , induced norm  $\|\cdot\|_{\mathcal{H}} := \langle \cdot \mid \cdot \rangle_{\mathcal{H}}^{1/2}$ , and a feature mapping  $\varphi: \mathcal{Z} \rightarrow \mathcal{H}: z \mapsto \varphi(z)$ , so that the celebrated *reproducing property* holds true:  $\forall Q^{(n)} \in \mathcal{H}, \forall z \in \mathcal{Z}, Q^{(n)}(z) = \langle Q^{(n)} \mid \varphi(z) \rangle_{\mathcal{H}}$  [26], [27]. To use familiar notations from linear algebra, the “dot-product”  $Q^{(n)\top} \varphi(z) =$

$\varphi^\top(\mathbf{z})Q^{(n)} := \langle Q^{(n)} | \varphi(\mathbf{z}) \rangle_{\mathcal{H}}$  will be used for the inner product hereafter, where  $\top$  stands for the transposition operator. To simplify notation for the distributed setting, let  $\Omega := [Q^{(1)}, \dots, Q^{(N)}] \in \mathcal{H}$ , where  $\mathcal{H}$  stands for the  $N$ -times Cartesian product space  $\mathcal{H} \times \dots \times \mathcal{H}$ , with inner product:  $\langle \Omega_1 | \Omega_2 \rangle_{\mathcal{H}} := \sum_{n=1}^N \langle Q_1^{(n)} | Q_2^{(n)} \rangle_{\mathcal{H}}$ ,  $\forall \Omega_1, \Omega_2 \in \mathcal{H}$ . For convenience, we use square brackets  $[\cdot]$  instead of parentheses  $(\cdot)$  to denote tuples  $\Omega$  in  $\mathcal{H}$ , allowing for the use of familiar linear algebra operations in the following sections.

### B. General assumptions for the decentralized setting

The following assumptions will serve as overarching assumptions throughout the discussion.

#### Assumptions 1.

- (i) **(Graph topology)** Graph  $\mathcal{G} := (\mathcal{N}, \mathcal{E})$  is connected [30]. Each agent  $n$  exchanges information only with its neighbors  $\mathcal{N}(n)$ , and there is no central master node collecting all information, meaning a “star topology” is not assumed.
- (ii) **(Common environment)** All agents interact with a shared environment  $(\mathcal{S}, \mathcal{A}, g)$ , where the state space  $\mathcal{S}$  is continuous, and the action space  $\mathcal{A}$  is discrete with finite cardinality.
- (iii) **(Trajectory-data-based learning)** Agents lack statistical knowledge required to compute  $\mathbb{E}_{s'|z}\{\cdot\}$  in (1). Instead, each agent  $n$  relies on its own trajectory data:

$$\mathcal{T}^{(n)} := \{ (s_i^{(n)}, a_i^{(n)}, g_i^{(n)}, s_i^{(n)'} = s_{i+1}^{(n)}) \}_{i=1}^{N_{\text{av}}^{(n)}},$$

for some positive integer  $N_{\text{av}}^{(n)}$ . The datasets  $\mathcal{T}^{(n)}$  and  $\mathcal{T}^{(n')}$  do not need to be identical, even partially, for any  $n, n' \in \mathcal{N}$ . Agents are not required to share any information about their state vectors.

- (iv) **(Q-function sharing)** Each agent  $n$  shares a copy of its Q-function  $Q^{(n)}$  with its neighbors  $\mathcal{N}_n$ .

As per Assumptions 1, agents must rely on trajectory data samples and cooperation to collectively approximate a fixed point of  $T_\diamond$  by seeking consensus. In decentralized fitted Q-iteration [24], for example, sequence  $(\Omega[k] := [Q^{(1)}[k], \dots, Q^{(N)}[k]])_{k \in \mathbb{N}}$  is generated according to VI [2]:

$$\Omega[k+1] := \mathbf{T}_{\text{TD}}(\Omega[k]), \quad (3)$$

so that  $(\Omega[k])_{k \in \mathbb{N}}$  converges, as  $k \rightarrow \infty$ , to a fixed point of the consensus-based Bellman mapping  $\mathbf{T}_{\text{TD}}: \mathcal{H} \rightarrow \mathcal{C}_{\mathcal{H}}: \Omega \mapsto \mathbf{T}_{\text{TD}}(\Omega)$ , defined as

$$\mathbf{T}_{\text{TD}}(\Omega) \in \arg \min_{\Omega' \in \mathcal{C}_{\mathcal{H}}} \sum_{n \in \mathcal{N}} \mathcal{L}_{\text{TD}}^{(n)}(Q^{(n)'}; Q^{(n)}), \quad (4)$$

where the classical temporal-difference (TD) loss

$$\begin{aligned} \mathcal{L}_{\text{TD}}^{(n)}(Q^{(n)'}; Q^{(n)}) \\ := \frac{1}{2} \sum_{i=1}^{N_{\text{av}}^{(n)}} \left[ g_i^{(n)} + \alpha \inf_{a_i^{(n)'} \in \mathcal{A}} Q^{(n)}(s_i^{(n)'}, a_i^{(n)'}) - Q^{(n)'}(z_i^{(n)}) \right]^2, \end{aligned}$$

and the *consensus set*

$$\begin{aligned} \mathcal{C}_{\mathcal{H}} &:= \{ \Omega' \in \mathcal{H} \mid Q^{(n)'} = Q^{(n')'}, \forall \{n, n'\} \in \mathcal{E} \} \\ &= \{ \Omega' \in \mathcal{H} \mid Q^{(1)'} = \dots = Q^{(N)'} \}, \end{aligned} \quad (5)$$

with the latter expression of  $\mathcal{C}_{\mathcal{H}}$  in (5) following from Assumption 1(i) that  $\mathcal{G}$  is connected [30].

As per Assumption 1(i), the summation in (4) cannot be computed locally by any node in  $\mathcal{G}$ , necessitating the use of a distributed algorithm. Works [18], [17], [23], [22], [16] follow a route similar to the previous setting and [24], whereas [20], [21] do not adopt Assumption 1(i) but consider a star topology for  $\mathcal{G}$ . Additionally, [18], [17], [22], [16], [20], [21] bypass Assumption 1(iii), focus on streaming/online data, and operate in online-learning and stochastic-optimization modes.

In MARL, it is often the case, e.g., [22], that each agent  $n$  possesses its own one-step loss function  $g^{(n)}(\cdot)$ , without knowledge of the losses of other agents. This contrasts with Assumption 1(ii). A network-wide one-step loss is then defined as  $g(\cdot) := (1/N) \sum_{n \in \mathcal{N}} g^{(n)}(\cdot)$ . Furthermore, it is also common in MARL for all agents to share their state vectors [19], [23], [24], [22], [21], which contrasts with Assumption 1(iii).

In addition to the proposed nonparametric B-Maps in Section III, and to expand the set of benchmark algorithms for validating the proposed VI Algorithm 1 in Section IV, this work introduces also a distributed approach for solving (4) using the well-known alternating direction method of multipliers (ADMM) [31].

### III. NOVEL DISTRIBUTED NONPARAMETRIC B-MAPS

#### A. The centralized (star-topology) B-Map

Has there been a *centralized fusion center*  $n_\star \in \mathcal{N}$ , connected with every node of  $\mathcal{G}$  (*star topology*), able to gather *all* data  $\{\mathcal{T}^{(n)}\}_{n \in \mathcal{N}}$  of Assumption 1(iii) and to perform all necessary computations, then, motivated by the nonparametric design of [12, (3b)], a star-topology B-Map  $T_\star: \mathcal{H} \rightarrow \mathcal{H}: Q \mapsto T_\star(Q)$  could be defined as

$$\begin{aligned} T_\star(Q) &:= \sum_{n \in \mathcal{N}} \sum_{i=1}^{N_{\text{av}}^{(n)}} \overbrace{[g_i^{(n)} + \alpha \inf_{a_i^{(n)'} \in \mathcal{A}} Q(s_i^{(n)'}, a_i^{(n)'})]}^{c_i^{(n)}(Q)} \psi_i^{(n)} \\ &:= \sum_{n \in \mathcal{N}} \Psi_\star^{(n)} c^{(n)}(Q), \end{aligned} \quad (6)$$

where

$$\begin{aligned} g_i^{(n)} &:= g(z_i^{(n)}) = g(s_i^{(n)}, a_i^{(n)}), \\ c^{(n)}(Q) &:= [c_1^{(n)}(Q), \dots, c_{N_{\text{av}}^{(n)}}^{(n)}(Q)]^\top, \\ \Psi_\star^{(n)} &:= [\psi_{\star 1}^{(n)}, \dots, \psi_{\star N_{\text{av}}^{(n)}}^{(n)}], \end{aligned}$$

and  $\{\{\psi_{\star i}^{(n)}\}_{i=1}^{N_{\text{av}}^{(n)}}\}_{n \in \mathcal{N}}$  are user-defined functions in  $\mathcal{H}$ . The B-Map in (6) serves as a surrogate of the classical (1) in cases where the computation of the conditional expectation in (1) is infeasible; see Assumption 1(iii). The conditional expectation in (1) is approximated in (6) by a linear combination of the user-defined  $\{\psi_{\star i}^{(n)}\} \subset \mathcal{H}$  with coefficients  $c_i^{(n)}(Q^{(n)})$ , defined by evaluations of the one-step  $g$  and the long-term Q-functions at  $\{\mathcal{T}^{(n)}\}_{n \in \mathcal{N}}$ .

The benefits of the design freedom offered by  $\{\psi_{\star i}^{(n)}\}$  have been already demonstrated in [12], where properly chosen

$\{\psi_{*i}^{(n)}\}$  yield well-known B-Map designs. Nevertheless, for a concrete discussion and motivated by [12], this study considers

$$\Psi_{*}^{(n)} := (\sum_{n \in \mathcal{N}} \Phi^{(n)} \Phi^{(n)\top} + \sigma \text{Id})^{-1} \Phi^{(n)} \quad (7a)$$

$$= (\Phi_{\mathcal{N}} \Phi_{\mathcal{N}}^{\top} + \sigma \text{Id})^{-1} \Phi^{(n)}, \quad (7b)$$

where

$$\Phi^{(n)} := [\varphi(\mathbf{z}_1^{(n)}), \dots, \varphi(\mathbf{z}_{N_{\text{av}}^{(n)}}^{(n)})],$$

$$\Phi^{(n)} \Phi^{(n)\top} = \sum_{i=1}^{N_{\text{av}}^{(n)}} \varphi(\mathbf{z}_i^{(n)}) \varphi^{\top}(\mathbf{z}_i^{(n)}), \quad (7c)$$

$$\Phi_{\mathcal{N}} := [\Phi^{(1)}, \dots, \Phi^{(N)}],$$

$$\Phi_{\mathcal{N}} \Phi_{\mathcal{N}}^{\top} = \sum_{n \in \mathcal{N}} \Phi^{(n)} \Phi^{(n)\top}, \quad (7d)$$

$\text{Id}: \mathcal{H} \rightarrow \mathcal{H}$  is the identity operator, and  $\sigma \in \mathbb{R}_{++}$ . Borrowing from the signal-processing jargon, (7c) will be called the *nodal covariance operator*, while (7d) the *network-wide covariance operator*. Notice that (7c) and (7d) operate in the feature space  $\mathcal{H}$ . Now, (6) takes the following special form via (7b):

$$\begin{aligned} T_{*}(Q) &= \sum_{n \in \mathcal{N}} \Psi_{*}^{(n)} \mathbf{c}^{(n)}(Q) \\ &= \sum_{n \in \mathcal{N}} (\Phi_{\mathcal{N}} \Phi_{\mathcal{N}}^{\top} + \sigma \text{Id})^{-1} \Phi^{(n)} \mathbf{c}^{(n)}(Q) \\ &= (\Phi_{\mathcal{N}} \Phi_{\mathcal{N}}^{\top} + \sigma \text{Id})^{-1} \Phi_{\mathcal{N}} \mathbf{c}_{\mathcal{N}}(Q) \\ &= \Phi_{\mathcal{N}} (\mathbf{K}_{\mathcal{N}} + \sigma \text{Id})^{-1} \mathbf{c}_{\mathcal{N}}(Q), \end{aligned} \quad (8)$$

where  $\mathbf{c}_{\mathcal{N}}(Q) := [\mathbf{c}^{(1)\top}(Q), \dots, \mathbf{c}^{(N)\top}(Q)]^{\top}$ ,  $\mathbf{K}_{\mathcal{N}} := \Phi_{\mathcal{N}}^{\top} \Phi_{\mathcal{N}}$ , and where  $(\Phi_{\mathcal{N}} \Phi_{\mathcal{N}}^{\top} + \sigma \text{Id})^{-1} \Phi_{\mathcal{N}} = \Phi_{\mathcal{N}} (\Phi_{\mathcal{N}}^{\top} \Phi_{\mathcal{N}} + \sigma \text{Id})^{-1} = \Phi_{\mathcal{N}} (\mathbf{K}_{\mathcal{N}} + \sigma \text{Id})^{-1}$  can be easily verified.

## B. Distributing the centralized B-Map

In the absence of a centralized fusion center (Assumption 1(i)), the computation of  $T_{*}$  in (6) is infeasible. Consequently, the following bottlenecks should be surmounted.

### Bottlenecks 2.

- (i) **(Q-function consensus)** Run a consensus-based distributed algorithm across  $\mathcal{G}$  to approximate the centralized computation of  $\sum_{n \in \mathcal{N}} \Psi_{*}^{(n)} \mathbf{c}^{(n)}(\cdot)$  in (6).
- (ii) **(Covariance-matrix consensus)** Run a consensus-based distributed algorithm across  $\mathcal{G}$  to approximate the network-wide covariance operator (7d), needed to define  $\Psi_{*}^{(n)}$  in (7b).
- (iii) **(Curse of dimensionality)** Due to the possible infinite dimensionality of  $\mathcal{H}$ , addressing Bottlenecks 2(i) and 2(ii) requires sharing high- or even infinite-dimensional objects, such as Q-functions and covariance operators, posing significant challenges to communication bandwidth constraints.

To surmount Bottlenecks 2, define first the following *nodal* B-Maps:  $T^{(n)}: \mathcal{H} \rightarrow \mathcal{H}: Q \mapsto T^{(n)}(Q)$  with

$$\begin{aligned} T^{(n)}(Q) &:= \sum_{i=1}^{N_{\text{av}}^{(n)}} [g_i^{(n)} + \alpha \inf_{a_i^{(n)'} \in \mathcal{A}} Q(s_i^{(n)'}, a_i^{(n)'})] \psi_i^{(n)} \\ &= \Psi^{(n)} \mathbf{c}^{(n)}(Q), \end{aligned} \quad (9)$$

where  $\Psi^{(n)} := [\psi_1^{(n)}, \dots, \psi_{N_{\text{av}}^{(n)}}^{(n)}]$  and  $\{\{\psi_i^{(n)}\}_{i=1}^{N_{\text{av}}^{(n)}}\}_{n \in \mathcal{N}}$  are user-defined functions in  $\mathcal{H}$ . Notice that since  $\mathcal{A}$  is finite according to Assumption 1(ii), the inf in (9) becomes min. To facilitate notations, gather all nodal B-Maps into the following *in-network* B-Map:  $\mathbf{T}: \mathcal{H} \rightarrow \mathcal{H}: \Omega = [Q^{(1)}, \dots, Q^{(N)}] \mapsto \mathbf{T}(\Omega)$  with

$$\mathbf{T}(\Omega) := [T^{(1)}(Q^{(1)}), \dots, T^{(N)}(Q^{(N)})]. \quad (10)$$

To address Bottleneck 2(i), this paper's counter-proposition to the consensus-based B-Map (4) is to solve distributively

$$\left[ \sum_{n \in \mathcal{N}} T^{(n)}(Q^{(n)}), \dots, \sum_{n \in \mathcal{N}} T^{(n)}(Q^{(n)}) \right] \quad (11a)$$

$$= [\mathbf{T}(\Omega) \mathbf{1}_N, \dots, \mathbf{T}(\Omega) \mathbf{1}_N]$$

$$= \arg \min_{\Omega' \in \mathcal{C}_{\mathcal{H}}} \sum_{n \in \mathcal{N}} \frac{1}{2} \|Q^{(n)'} - N T^{(n)}(Q^{(n)})\|_{\mathcal{H}}^2$$

$$= \arg \min_{\Omega' \in \mathcal{C}_{\mathcal{H}}} \frac{1}{2} \|\Omega' - N \mathbf{T}(\Omega)\|_{\mathcal{H}}^2, \quad (11b)$$

by using the framework of [32], selected because of its generality, flexibility, and simple form of recursions. Define now the linear operators  $A^Q, A_{\varpi}^Q: \mathcal{H} \rightarrow \mathcal{H}$  by

$$A^Q(\Omega) := \Omega(\mathbf{I}_N - \gamma \mathbf{L}), \quad (12a)$$

$$A_{\varpi}^Q(\Omega) := \varpi A^Q(\Omega) + (1 - \varpi) \Omega, \quad (12b)$$

$\forall \Omega \in \mathcal{H}$ . In (12),  $\varpi \in [1/2, 1)$ , the graph Laplacian matrix  $\mathbf{L} := \text{diag}(\mathbf{W} \mathbf{1}_N) - \mathbf{W}$  [33], with the  $N \times N$  adjacency matrix  $\mathbf{W} = [w_{nn'}]$  defined as  $w_{nn'} := 1$ , if  $\{n, n'\} \in \mathcal{E}$ ,  $w_{nn'} := 0$ , if  $\{n, n'\} \notin \mathcal{E}$ , and  $w_{nn} := 0$ ,  $\forall n \in \mathcal{N}$ . Further,  $\text{diag}(\cdot)$  transforms a vector into a diagonal matrix with the entries of the vector placed at the main diagonal of the matrix, and  $\mathbf{1}_N$  is the  $N \times 1$  all-one vector. Additionally,  $\gamma \in (0, 1/\|\mathbf{L}\|_2]$ , where  $\|\mathbf{L}\|_2$  is the spectral norm of  $\mathbf{L}$  [34].

Owing to the definition of the Laplacian matrix, notice that the  $n$ th entry of  $A^Q(\Omega)$  in (12a) takes the following form:

$$(A^Q(\Omega))^{(n)} = (1 - \gamma |\mathcal{N}_n|) Q^{(n)} + \gamma \sum_{n' \in \mathcal{N}_n} Q^{(n')}. \quad (13)$$

This is a clear demonstration of the distributive nature of  $A^Q$ , because not only the local Q-function  $Q^{(n)}$  but also copies of  $\{Q^{(n')}\}_{n' \in \mathcal{N}_n}$  need to be transmitted from neighbors  $\mathcal{N}_n$  to node  $n$  to compute  $(A^Q(\Omega))^{(n)}$ . Because of  $\gamma \in (0, 1/\|\mathbf{L}\|_2]$ , it can be verified that  $\|A^Q\| = \|\mathbf{I}_N - \gamma \mathbf{L}\|_2 \leq 1$ , where  $\|A^Q\|$  is the norm induced by the inner product  $\langle \cdot | \cdot \rangle_{\mathcal{H}}$ . Moreover, because  $\gamma \leq 1/\|\mathbf{L}\|_2$ , it can be verified that  $\langle A^Q(\Omega) | \Omega \rangle_{\mathcal{H}} \geq 0$ ,  $\forall \Omega \in \mathcal{H}$ , that is,  $A^Q$  is positive [35, §9.3]. Now, notice that  $\mathbf{L} \mathbf{1}_N = \mathbf{0} = 0 \cdot \mathbf{1}_N$ . By Assumption 1(i) and the fact that  $\mathbf{L}$  is positive semidefinite [33, Lem. 4.3], the rank of  $\mathbf{L}$  is  $N - 1$  with 0 being its smallest eigenvalue, and the kernel space  $\ker \mathbf{L} = \text{span}(\mathbf{1}_N)$ , so that

$$\text{Fix}(A^Q) := \{\Omega \in \mathcal{H} \mid A^Q(\Omega) = \Omega\} = \mathcal{C}_{\mathcal{H}}. \quad (14)$$

As in (3),  $k \in \mathbb{N}$  serves as the VI index in this paper; see Figure 1. With  $\Omega[k] = [Q^{(1)}[k], \dots, Q^{(N)}[k]] \in \mathcal{H}$  being the snapshot of all Q-function estimates across  $\mathcal{G}$  at VI iteration  $k$ , the aforementioned properties of  $A^Q$  and (14) ensure that the sequence  $(\Omega_m[k])_{m \in \mathbb{N}}$  generated by  $\Omega_{-1}[k] := [0, \dots, 0]$  and,  $\forall m \in \mathbb{N}$ ,

$$\Omega_0[k] := A_{\varpi}^Q(\Omega_{-1}[k]) - \eta(\Omega_{-1}[k] - N \mathbf{T}(\Omega[k])), \quad (15a)$$

$$\begin{aligned} \mathfrak{Q}_{m+1}[k] &:= \mathfrak{Q}_m[k] - (A_\varpi^Q(\mathfrak{Q}_{m-1}[k]) - \eta \mathfrak{Q}_{m-1}[k]) \\ &\quad + (A^Q(\mathfrak{Q}_m[k]) - \eta \mathfrak{Q}_m[k]), \end{aligned} \quad (15b)$$

with  $\eta \in (0, 2(1 - \varpi))$ , converges strongly (recall that  $\mathcal{H}$  may be infinite dimensional) to the solution (11a) as  $m \rightarrow \infty$  [32, Lem. 3.4 and Cor. 3.5]. Even more, a linear convergence rate for  $(\mathfrak{Q}_m[k])_{m \in \mathbb{N}}$  is established by Theorem 5(ii).

Bottleneck 2(iii) appears prominently in the previous discussion, because possibly infinite dimensional Q-functions need to be shared among neighbors to compute (13). To surmount Bottleneck 2(iii), dimensionality reduction is needed. To this end, the feature mapping  $\varphi: \mathcal{Z} \rightarrow \mathcal{H}$  will be replaced henceforth by the random-Fourier-feature-(RFF) mapping [29]  $\tilde{\varphi}: \mathcal{Z} \rightarrow \mathbb{R}^D: \mathbf{z} \mapsto \tilde{\varphi}(\mathbf{z})$ , for a user-defined  $D \in \mathbb{N}_*$ , with

$$\tilde{\varphi}(\mathbf{z}) := \sqrt{\frac{2}{D}} [\cos(\mathbf{v}_1^\top \mathbf{z} + u_1), \dots, \cos(\mathbf{v}_D^\top \mathbf{z} + u_D)]^\top, \quad (16)$$

where  $\{\mathbf{v}_i\}_{i=1}^D$  and  $\{u_i\}_{i=1}^D$  are samples from the Gaussian and uniform distributions, respectively. In other words, Q-functions in  $\mathcal{H}$  are approximated by  $D$ -dimensional representations, where a larger  $D$  yields more accurate approximations. Although  $\tilde{\varphi}$  replaces  $\varphi$ ,  $\varphi$  will continue to be used for clarity and simplicity, with the understanding that  $\tilde{\varphi}$  is implemented behind the scenes.

Drawing now attention to Bottleneck 2(ii), a distributed scheme is needed to compute the  $D \times D$  network-wide covariance matrix  $\Phi_{\mathcal{N}} \Phi_{\mathcal{N}}^\top$  of (7d); recall that the RFF  $\tilde{\varphi}$  is implemented now in computations. To this end, define the linear vector space of operators  $\mathcal{O} := \mathbb{R}^{D \times ND} = \{\mathfrak{C} := [\mathbf{C}^{(1)}, \dots, \mathbf{C}^{(N)}] \mid \mathbf{C}^{(n)} \in \mathbb{R}^{D \times D}\}$ , equipped with the standard inner product  $\langle \mathfrak{C}_1 \mid \mathfrak{C}_2 \rangle_{\mathcal{O}} := \text{trace}(\mathfrak{C}_1^\top \mathfrak{C}_2)$ ,  $\forall \mathfrak{C}_1, \mathfrak{C}_2 \in \mathcal{O}$ . Observe then

$$[\Phi_{\mathcal{N}} \Phi_{\mathcal{N}}^\top, \dots, \Phi_{\mathcal{N}} \Phi_{\mathcal{N}}^\top] \quad (17a)$$

$$= \arg \min_{\mathfrak{C} \in \mathcal{O}} \sum_{n \in \mathcal{N}} \frac{1}{2} \|\mathbf{C}^{(n)} - N \Phi^{(n)} \Phi^{(n)\top}\|_{\text{F}}^2,$$

$$= \arg \min_{\mathfrak{C} \in \mathcal{O}} \frac{1}{2} \|\mathfrak{C} - N \mathfrak{C}_{\mathcal{N}}\|_{\text{F}}^2, \quad (17b)$$

where  $\|\cdot\|_{\text{F}}$  is the Frobenius norm,

$$\mathfrak{C}_{\mathcal{N}} := [\Phi^{(1)} \Phi^{(1)\top}, \dots, \Phi^{(N)} \Phi^{(N)\top}] \quad (18)$$

gathers all nodal covariance operators, and the consensus set

$$\begin{aligned} \mathcal{C}_{\mathcal{O}} &:= \{\mathfrak{C} \in \mathcal{O} \mid \mathbf{C}^{(n)} = \mathbf{C}^{(n')}, \forall \{n, n'\} \in \mathcal{E}\} \\ &= \{\mathfrak{C} \in \mathcal{O} \mid \mathbf{C}^{(1)} = \dots = \mathbf{C}^{(N)}\}. \end{aligned}$$

Along the lines of (12), define the linear operators  $A^C, A_\varpi^C: \mathcal{O} \rightarrow \mathcal{O}$  by

$$A^C(\mathfrak{C}) := \mathfrak{C} (\mathbf{I}_N - \gamma \mathbf{L}) \otimes \mathbf{I}_D, \quad (19a)$$

$$A_\varpi^C(\mathfrak{C}) := \varpi A^C(\mathfrak{C}) + (1 - \varpi) \mathfrak{C}, \quad (19b)$$

$\forall \mathfrak{C} \in \mathcal{O}$ , where  $\otimes$  stands for the Kronecker product,  $\gamma \in (0, 1/\|\mathbf{L}\|_2]$ , and  $\varpi \in [1/2, 1)$ . It is not difficult to verify that per node  $n$ , only  $\mathbf{C}^{(n)}$  and copies of  $\{\mathbf{C}^{(n')}\}_{n' \in \mathcal{N}_n}$  from the neighboring agents need to be shared to compute

$$(A^C(\mathfrak{C}))^{(n)} = (1 - \gamma|\mathcal{N}_n|) \mathbf{C}^{(n)} + \gamma \sum_{n' \in \mathcal{N}_n} \mathbf{C}^{(n')}. \quad (20)$$

Moreover, similarly to the discussion following (13) and by using basic properties of  $\otimes$ , it can be verified that  $\|A^C\| = \|(\mathbf{I}_N - \gamma \mathbf{L}) \otimes \mathbf{I}_D\|_2 = \|\mathbf{I}_N - \gamma \mathbf{L}\|_2 \leq 1$ , that  $A^C$  is positive, that  $(\mathbf{L} \otimes \mathbf{I}_D)(\mathbf{1}_N \otimes \mathbf{I}_D) = (\mathbf{L} \mathbf{1}_N) \otimes \mathbf{I}_D = \mathbf{0}$ , that  $\ker(\mathbf{L} \otimes \mathbf{I}_D) = \text{span}(\mathbf{1}_N \otimes \mathbf{I}_D)$ , and that

$$\text{Fix}(A^C) := \{\mathfrak{C} \in \mathcal{O} \mid A^C(\mathfrak{C}) = \mathfrak{C}\} = \mathcal{C}_{\mathcal{O}}. \quad (21)$$

Consequently, and similarly to (15), sequence  $(\mathfrak{C}_l = (\mathbf{C}_l^{(1)}, \dots, \mathbf{C}_l^{(N)}))_{l \in \mathbb{N}}$  generated by  $\mathfrak{C}_{-1} := (\mathbf{0}, \dots, \mathbf{0})$  and

$$\mathfrak{C}_0 := A_\varpi^C(\mathfrak{C}_{-1}) - \eta(\mathfrak{C}_{-1} - N \mathfrak{C}_{\mathcal{N}}), \quad (22a)$$

$$\begin{aligned} \mathfrak{C}_{l+1} &:= \mathfrak{C}_l - (A_\varpi^C(\mathfrak{C}_{l-1}) - \eta \mathfrak{C}_{l-1}) \\ &\quad + (A^C(\mathfrak{C}_l) - \eta \mathfrak{C}_l), \end{aligned} \quad (22b)$$

$\forall l \in \mathbb{N}$ , with  $\eta \in (0, 2(1 - \varpi))$ , converges to the solution (17a), that is, for any node  $n$ ,  $\lim_{l \rightarrow \infty} \mathbf{C}_l^{(n)} = \Phi_{\mathcal{N}} \Phi_{\mathcal{N}}^\top$  [32, Lem. 3.4 and Cor. 3.5]. Refer to Theorem 5(iii) for a stronger result on the linear convergence rate of the sequence of estimates.

The aforementioned arguments are consolidated in Algorithm 1. To establish the connection between (15), (22), and VI, note that any index  $l$  of (22) can be expressed as  $l = kM + m$  (see line 10 of Algorithm 1), where  $m \in \{0, 1, \dots, M-1\}$  is the index of (15), and  $k$  is the VI index. This observation emphasizes that (15), which aims to achieve consensus among Q-functions across  $\mathcal{G}$ , runs only  $M$  times between two consecutive VI indices (see lines 8–16 of Algorithm 1 and Figure 1). Agent  $n$  runs iteration (22) in parallel with (15). To conserve computational resources and communication bandwidth, Algorithm 1 allows the update in (22) to be implemented once every  $J_C$  iterations ( $\mathbb{N}_* \ni J_C \leq M$ ); see lines 11–15 of Algorithm 1. The effect of  $J_C$  on the performance of Algorithm 1 is explored in Figures 3(b) and 4(b). Iteration (22) provides (15) with estimates  $\mathbf{C}_{l=kM}^{(n)}$  through the following update of the nodal basis vectors  $\Psi^{(n)}[k]$  at VI iteration  $k$ :

$$\Psi^{(n)}[k] := (\mathbf{C}_{kM}^{(n)} + \sigma \mathbf{I}_D)^{-1} \Phi^{(n)}. \quad (23)$$

To justify (23) recall from the discussion after (22) that for all sufficiently large values of  $k$ , the covariance-matrix estimate  $\mathbf{C}_{kM}^{(n)}$  lies very close to  $\Phi_{\mathcal{N}} \Phi_{\mathcal{N}}^\top$ . Notice also that the adoption of (23) in (9) makes  $T^{(n)}$  dependent on index  $k$ . To avoid overloading notations with indices,  $k$  will be omitted from  $T^{(n)}$  hereafter.

It is clear from the previous discussion that, in addition to the general Assumptions 1 and in contrast to most prior DRL schemes, Algorithm 1 also adopts the following assumption.

**Assumption 3. (Covariance-matrix sharing)** In Algorithm 1, agent  $n$  communicates a copy of its covariance-matrix estimate  $\mathbf{C}_{kM}^{(n)}$  to its neighbors  $\mathcal{N}_n$ .

Actually, since  $\mathbf{C}_{kM}^{(n)}$  is symmetric, only  $D(D+1)/2$  real-valued entries of  $\mathbf{C}_{kM}^{(n)}$  need to be transmitted to the neighbors  $\mathcal{N}_n$ . Nonetheless, Algorithm 1 theoretically requires more communication bandwidth to operate compared to DRL designs that adhere only to Assumption 1(iv). Surprisingly, the numerical tests in Section IV reveal the opposite: Algorithm 1 consumes less cumulative communication bandwidth

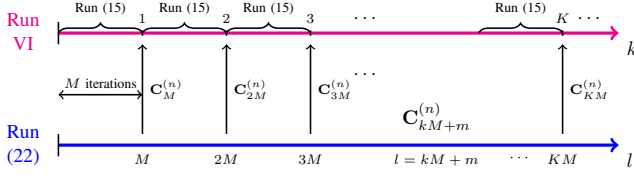


**Fig. 1:** Iteration (22) is implemented to provide consensual estimates of the network-wide covariance operator (7d), while (15) provides consensual estimates of the fixed point  $Q_*$  of the star-topology B-Map (6). Iteration (22) feeds the covariance-operator estimate  $\mathbf{C}_{kM}^{(n)}$  to iteration (15) periodically ( $l = kM$ ). This estimate is needed to define the nodal basis vectors in (23) at VI index  $k$ ; see line 5 of Algorithm 1. Iteration (15) runs only  $M$  times between two consecutive VI indices.

### Algorithm 1 Distributed value iteration (VI)

**Input:** Graph  $\mathcal{G} = (\mathcal{N}, \mathcal{E})$ , data  $\{\mathcal{T}^{(n)}\}_{n \in \mathcal{N}}$ , reproducing kernel  $\kappa$ ,  $\varpi \in [1/2, 1)$ ,  $\eta \in (0, 2(1 - \varpi))$ ,  $\gamma \in (0, 1/\|\mathbf{L}\|_2]$ ,  $M \in \mathbb{N}_*$ ,  $J_C \in \{1, \dots, M\}$ .

**Output:**  $(\Omega[k] = (Q^{(1)}[k], \dots, Q^{(N)}[k]))_{k \in \mathcal{N}}$

- 1: Define  $\mathcal{C}_{\mathcal{N}}$  by (18).
- 2: Set  $\mathcal{C}_{-1} := [0, \dots, 0]$ . Compute  $\mathcal{C}_0$  by (22a).
- 3: **for**  $k = 0, 1, \dots, \infty$  **do**
- 4: Estimates  $\mathcal{C}_{kM} = (\mathbf{C}_{kM}^{(1)}, \dots, \mathbf{C}_{kM}^{(N)})$  are available to the agents.
- 5: Compute  $\{\Psi^{(n)}[k]\}_{n=1}^N$  by (23).
- 6: Compute  $\mathbf{T}(\Omega[k])$  by (10).
- 7: Set  $\Omega_{-1}[k] := \Omega[k]$ . Compute  $\Omega_0[k]$  by (15a).
- 8: **for**  $m = 0, 1, \dots, M - 1$  **do** \\* Run (15b)  $M$  times \\*
- 9: Compute  $\Omega_{m+1}[k]$  by (15b).
- 10: Define index  $l := kM + m$ .
- 11: **if**  $(m \bmod J_C) = 0$  **then**
- 12: \\* Run (22b) once every  $J_C$  times: \\*  
Compute  $\mathcal{C}_{l+1}$  by (22b).
- 13: **else**
- 14: Set  $\mathcal{C}_{l+1} := \mathcal{C}_l$  and  $\mathcal{C}_l := \mathcal{C}_{l-1}$ .
- 15: **end if**
- 16: **end for**
- 17:  $\Omega[k+1] := \Omega_M[k]$ . \\* VI update \\*
- 18: **end for**

to converge than prior-art DRL designs that follow only Assumption 1(iv); see Figures 3(a) and 4(a).

### C. Performance analysis of Algorithm 1

First, consider the eigenvalue decomposition (EVD) of the Laplacian matrix  $\mathbf{L} = \mathbf{U} \text{diag}(\lambda_1, \dots, \lambda_{N-1}, \lambda_N) \mathbf{U}^\top$ , where  $\|\mathbf{L}\|_2 = \lambda_1 \geq \dots \geq \lambda_{N-1} \geq \lambda_N \geq 0$ , and  $\mathbf{U}$  is orthogonal. Because of the connectedness of  $\mathcal{G}$  by Assumption 1(i),  $\lambda_{N-1} > \lambda_N = 0$  [33, Lem. 4.3]. Define then

$$b_n := \frac{\lambda_n}{\lambda_1}, \quad \forall n \in \{1, \dots, N\}, \quad (24)$$

so that  $1 = b_1 \geq b_2 \geq \dots \geq b_{N-1} > b_N = 0$ . Define also

$$\varrho(\eta) := \max \left\{ \max_{n \in \mathcal{N} \setminus \{N\}} \frac{|p_n + \sqrt{p_n^2 + 4q_n}|}{2}, (1 - \eta) \right\}, \quad (25a)$$

$$p_n := 2 - \eta - \gamma \lambda_n, \quad (25b)$$

$$q_n := \varpi \gamma \lambda_n + \eta - 1. \quad (25c)$$

### Assumptions 4.

- (i) Set  $\gamma := 1/\|\mathbf{L}\|_2 = 1/\lambda_1$  in Algorithm 1.
- (ii) The centralized B-Map  $T_*$  in (6) is a contraction [36], that is, Lipschitz continuous with coefficient  $\beta_* \in (0, 1)$  and  $\|T_*(Q_1) - T_*(Q_2)\| \leq \beta_* \|Q_1 - Q_2\|$ ,  $\forall Q_1, Q_2$ . Consequently, it is guaranteed that the fixed-point set of  $T_*$

is nonempty and a singleton:  $\text{Fix}(T_*) = \{Q \mid T_*(Q) = Q\} = \{Q_*\}$  [36].

- (iii) The Lipschitz coefficients  $(\beta^{(n)}[k])_{k \in \mathbb{N}}$  of the nodal B-Maps  $(T^{(n)} = T^{(n)}[k])_{k \in \mathbb{N}}$  in (9) (recall the discussion after (23)) are bounded.
- (iv) For any node  $n \in \mathcal{N}$ , sequence  $(Q^{(n)}[k])_{k \in \mathbb{N}}$  is bounded.
- (v) Let  $\varpi := 1/2$  in Algorithm 1.
- (vi) The  $b_{N-1}$  of (24) satisfies  $b_{N-1} \in (0, 1/2)$ .

Few comments are in order to justify the introduction of the previous assumptions. By following the arguments in the proof of Theorem 2 in [12], it can be demonstrated that both  $T_*$  in (6) and  $T^{(n)} = T^{(n)}[k]$  in (9) are Lipschitz continuous. A detailed discussion on conditions which ensure that the Lipschitz coefficient of  $T_*$  is strictly smaller than 1 (Assumption 4(ii)) can be found after Assumptions 3 in [12]. To save space, such a discussion and the related proofs are omitted. It is also worth recalling that the classical Bellman mapping  $T_\diamond$  in (1) is a well-known contraction (in a point-wise sense) [2], [1]. Assumption 4(iv) is used to ensure the existence of the constant  $C$  in (37). Assumption 4(vi) is taken as a premise to establish Lemmata 8 and 9, and to simplify the presentation by avoiding lengthy arguments and proofs in the general case where  $b_{N-1} \in (0, 1]$ . Similarly, Assumptions 4(i) and 4(vi) are introduced to simplify proofs.

The following theorem presents the main findings of the performance analysis. Theorem 5(ii) asserts that the nodal Q-functions estimates (steps 8–16 of Algorithm 1) converge to a consensual Q-function *linearly* [37, p. 619]. A similar result holds true for the covariance-matrix estimates in Theorem 5(iii). Moreover, Theorem 5(iv) states that for sufficiently large iteration VI indices  $k$ , the difference between the nodal Q-function estimate  $Q^{(n)}[k]$  and the fixed point  $Q_*$  of the centralized B-Map  $T_*$  can be made arbitrarily small, at a linear rate with respect to the parameter  $M$  of Algorithm 1. In simple terms, the longer the inner loop (steps 8–16 of Algorithm 1) runs, the closer the VI output  $Q^{(n)}[k]$  at node  $n$  is to  $Q_*$ . This clearly indicates that the proposed DRL design closely mirrors the behavior of a centralized fusion center.

**Theorem 5.** Presume Assumptions 1 and Assumption 4(i). The following hold true.

- (i)  $\forall \eta \in (0, 2(1 - \varpi))$ ,  $0 < \varrho(\eta) < 1$ .
- (ii) Let  $(\Omega_m[k] = [Q_m^{(1)}[k], \dots, Q_m^{(N)}[k]])_{m \in \mathbb{N}}$  be the sequence generated by (15). Then, for every node  $n \in \mathcal{N}$ ,

$$\|Q_m^{(n)}[k] - \mathbf{T}(\Omega[k]) \mathbf{1}_N\| = \mathcal{O}(m \varrho^m(\eta)),$$

where  $\mathbf{T}(\cdot)$  is defined by (10),  $\|\cdot\|$  stands for the Euclidean norm in  $\mathbb{R}^D$ , and  $\mathcal{O}(\cdot)$  is the classical big-oh notation [38].

- (iii) Let  $(\mathcal{C}_l = [\mathbf{C}_l^{(1)}, \dots, \mathbf{C}_l^{(N)}])$  be the sequence generated by (22), and  $\Phi_{\mathcal{N}} \Phi_{\mathcal{N}}^\top$  the network-wide covariance matrix of (7d). Then, for every node  $n \in \mathcal{N}$ ,

$$\|\mathbf{C}_l^{(n)} - \Phi_{\mathcal{N}} \Phi_{\mathcal{N}}^\top\|_F = \mathcal{O}(l \varrho^l(\eta)).$$

- (iv) Consider also Assumptions 4(ii) and 4(iv). Then, there exists  $C \in \mathbb{R}_{++}$  such that (s.t.)

$$\limsup_{k \rightarrow \infty} \|Q^{(n)}[k] - Q_*\| \leq C \frac{1}{1 - \beta_*} M \varrho^M(\eta),$$

where  $Q_*$  is the unique fixed point of the centralized B-Map  $T_*$  (Assumption 4(ii)).

*Proof:* See the appendix. ■

Interestingly, the following theorem states that the optimal learning rate  $\eta_*$  of recursions (15) and (22), which offers the “maximum” linear convergence rate in Theorem 5, is determined by the value  $b_{N-1}$  in (24).

**Theorem 6.** Consider Assumptions 4(i), 4(v) and 4(vi). Notice that under Assumption 4(v),  $\eta \in (0, 1)$ . Then,

$$\left(-b_{N-1} + \sqrt{2b_{N-1}}\right) =: \eta_* = \arg \min_{\eta \in (0,1)} \varrho(\eta).$$

*Proof:* See the appendix. ■

#### IV. NUMERICAL TESTS

To validate Algorithm 1, a network  $\mathcal{G}$  with  $N = 25$  nodes arranged on a  $5 \times 5$  orthogonal grid is used. Each agent is placed at a node  $n \in \{1, \dots, 25\}$  of  $\mathcal{G}$ , where agents communicate with their neighbors to the north, south, east, and west. Each of the 25 agents is assigned an independent system and learning task, resulting in a total of 25 systems. Two scenarios are considered: one where each system is a pendulum [39], [40], [41] (Section IV-A) and another where each system is a cartpole [39], [42] (Section IV-B); see Figure 2. The goal is for all agents to collaborate via the graph topology to efficiently complete their learning tasks with minimal communication cost.

Algorithm 1 competes against the following designs.

- (i) **(D-FQ)** The decentralized fitted Q-iteration (D-FQ) [24] solves the TD task (4). In its original form, [24] assumes that all agents share the same state information, i.e.,  $s_i^{(n)} = s_i^{(n')}$ , for all  $i$  and for all  $n, n' \in \mathcal{N}$  (global state space). However, since Assumption 1(iii) relaxes this constraint, allowing agents to keep their states private, [24] is adapted to the current setting by eliminating the assumption of a global state space.
- (ii) **(D-LSTD)** The diffusion off-policy gradient TD [18] efficiently minimizes, via stochastic gradient descent, a primal-dual reformulation of the widely used projected Bellman residual error (PBRE) encountered in the classical LSTD [2]. Due to the use of PBRE, the acronym D-LSTD will be used hereafter to refer to [18]. Originally, [18] was designed for J- and not Q-functions, and for online/streaming data. However, in the current setting, as described by Assumptions 1, where the data is fixed, each gradient-TD step of D-LSTD is performed using all the available data at agent  $n$  (batch processing), for a total of  $M$  steps, similar to Algorithm 1. Moreover, to robustify the original policy improvement of [18], the following running-average “smoothing” strategy is employed:  $\mu^{(n)}[k+1] = \argmin_{a \in \mathcal{A}} Q_{\text{smooth}}^{(n)}[k](s, a)$ , where  $Q_{\text{smooth}}^{(n)}[k] = 0.3 Q_{\text{smooth}}^{(n)}[k-1] + 0.7 Q^{(n)}[k]$ .
- (iii) **(Gossip-NN)** The Gossip-based [25], originally designed for general distributed learning tasks, can also be applied to the TD task (4), where a fully connected neural network (NN) serves as the nonlinear Q-function. Consequently, we refer to [25] as Gossip-NN hereafter. Notably,

the use of an NN makes Gossip-NN *parametric*, distinguishing it from the proposed nonparametric Algorithm 1.

- (iv) **(D-TD[ADMM])** An ADMM-based [31] solution to the TD task (4), proposed for the first time here to compete against [32] and its iterations in (15) and (22). Henceforth, D-TD[ADMM] will be used to denote this ADMM-based solution. The regularization term  $\sigma' \|Q^{(n)}\|_{\mathcal{H}}^2$ ,  $\sigma' \in \mathbb{R}_{++}$ , is also included in the loss  $\mathcal{L}_{\text{TD}}^{(n)}$  of (4) to mimic the regularization offered by  $\sigma$  in (23). D-TD[ADMM] employs also RFFs [see (16)] for dimensionality reduction.

The parameters for each method were carefully tuned, and the curves corresponding to the parameters that produced the “best” performance for each method are shown in the following figures. Each curve represents the uniformly averaged result of 100 independent tests.

In Algorithm 1,  $\sigma = 0.01$  in (23),  $M = 50$ , while  $\varpi = 0.5$ ,  $\gamma = 1/\|\mathbf{L}\|_2$  for the parameters of [32] in Algorithm 1, and  $\eta = -b_{N-1} + (2b_{N-1})^{1/2}$  according to Theorem 6. The discount factor  $\alpha = 0.9$  is used for all employed methods. Moreover, for all competitors of Algorithm 1, dimension  $D$  of the RFF approximating space is set as  $D = 500$  for Section IV-A, while  $D = 250$  for Section IV-B. Several values of  $D$  will be explored for Algorithm 1.

All employed methods run their distributed algorithm for  $M$  iterations between two consecutive value-iteration steps, as shown in Figure 1. The value of  $M$ , determined through extensive tuning, varies between methods and is listed in Table I. Note that Algorithm 1 uses the smallest value of  $M$ , as it requires fewer iterations than its competitors to reach consensus, as demonstrated in Figure 3(c) and Figure 4(c), and further supported by Theorem 5(ii).

Since each competing method uses different values for  $M$ , shares varying amounts of information among agents, and aims to minimize communication costs while achieving its objectives, the curves in Figures 3(a), 3(b), 4(a) and 4(b) are presented differently from the usual approach. Instead of plotting loss functions against VI iteration indices, each point on the curves represents the loss in relation to the cumulative communication cost (in bytes) used across  $\mathcal{G}$  at a specific VI iteration index  $k$ . Therefore, the closer a curve is to the left and bottom edges of the figure, the better the method’s performance.

TABLE I: Values of  $M$  per method and scenario

Method \ Scenario	Pendulum	Cartpole
D-FQ [24]	500	500
D-LSTD [18]	2500	2500
Gossip-NN [25]	1000	2000
D-TD[ADMM]	2000	2000
Algorithm 1	50	50

##### A. Network of pendulums

Each of the 25 agents is assigned a pendulum [39], [40], [41], for a total of 25 pendulums. One endpoint of each pendulum is fixed, while the other is free to move, as illustrated in Figure 2(a). At node  $n$  of  $\mathcal{G}$ , agent  $n$  applies torque to pendulum  $n$ , and by sharing information with neighboring



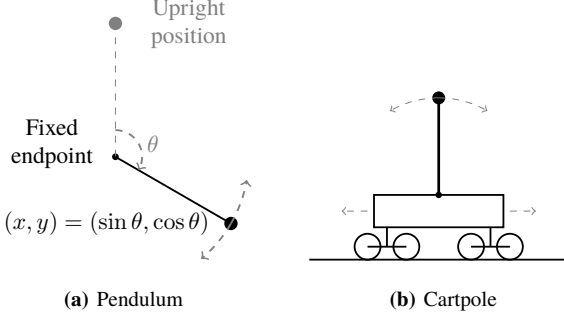


**Fig. 2:** Software for the pendulum and cartpole environments can be found in [40] and [42], respectively.

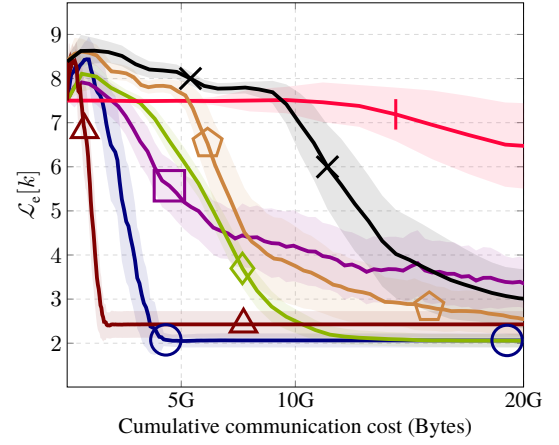
agents, the goal is for all pendulums to collectively swing from their bottom (rest) position to the upright position and remain there, with the minimal possible communication cost.

According to [39], the generic state at node  $n$  is defined as  $\mathbf{s}^{(n)} := [\sin \theta^{(n)}, \cos \theta^{(n)}, \dot{\theta}^{(n)}]^\top \in \mathcal{S} := \mathbb{R}^3$ , where  $\theta^{(n)}$  measures the angle between the current direction of the pendulum's arm and the upward direction,  $\dot{\theta}^{(n)}$  is the angular velocity, while torque serves as action  $a^{(n)} \in \mathcal{A}$ , with the action space  $\mathcal{A}$  defined as the finite grid resulting from evenly dividing  $[-2, 2]$  into 10 equal intervals. With the generic state-action vector defined as  $\mathbf{z}^{(n)} := [\mathbf{s}^{(n)\top}, a^{(n)}]^\top$ , the one-step loss function is defined as

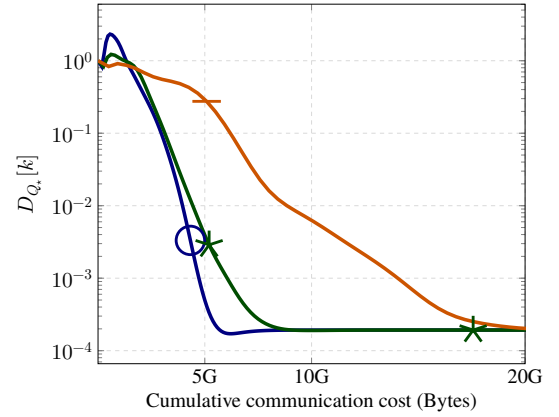
$$g(\mathbf{z}^{(n)}) := (\theta^{(n)})^2 + 0.1 (\dot{\theta}^{(n)})^2 + 0.001 (a^{(n)})^2.$$

The data trajectory  $\mathcal{T}^{(n)}$  of Assumption 1(iii) is generated inductively as follows: starting with a random  $\mathbf{s}_0^{(n)}$  as in [39], at state  $\mathbf{s}_i^{(n)}$ , action  $a_i^{(n)}$  is selected randomly from  $\mathcal{A}$ , and receives the one-step loss  $g_i^{(n)} = g(\mathbf{z}_i^{(n)})$  to transition to  $\mathbf{s}_{i+1}^{(n)} := \mathbf{s}_i^{(n)'}$ , according to a transition module function  $F_{\text{trans}}(\cdot)$ , inherent to the system [39], [40]. Although  $F_{\text{trans}}(\cdot)$  does not include any noise in its original design [39], to offer a more realistic setting here, measurement noise is also considered, so that  $(\theta_{i+1}^{(n)}, \dot{\theta}_{i+1}^{(n)}) = F_{\text{trans}}(\theta_i^{(n)} + \epsilon_1, \dot{\theta}_i^{(n)} + \epsilon_2, a_i^{(n)} + \epsilon_3)$ , where  $\epsilon_k$  is a random variable that follows the Gaussian PDF  $\mathcal{N}(0, \sigma_k)$ , with  $\sigma_1 = 0.05$ ,  $\sigma_2 = 0.25$ , and  $\sigma_3 = 0.05$ . This inductive construction of the trajectory continues till index  $i$  reaches the number  $N_{\text{av}}^{(n)} = 500$ .

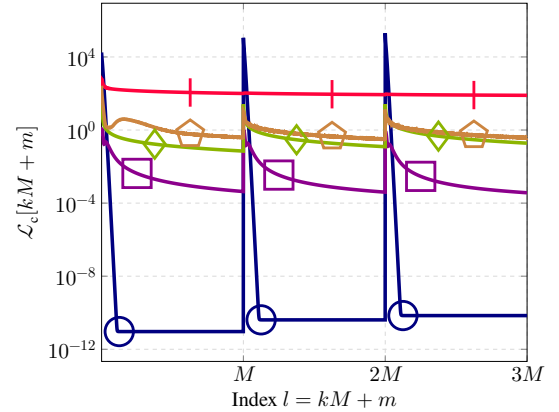
To validate the current estimate  $Q^{(n)}[k]$  of each one of the employed methods, *test* or *episodic* trajectory data  $\mathcal{E}_k := (\mathbf{s}_i^{(n)}[k], \mathbf{a}_i^{(n)}[k], \mathbf{s}_{i+1}^{(n)}[k])_{i=0}^{N_e-1}$ , for some  $N_e \in \mathbb{N}_*$ , are generated inductively as follows: starting from the pendulum's rest position  $\mathbf{s}_0^{(n)}[k] := [\sin \pi, \cos \pi, 0]^\top$ , and given  $\mathbf{s}_i^{(n)}[k]$ , apply torque  $\mathbf{a}_i^{(n)}[k] := \arg \min_{a \in \mathcal{A}} Q^{(n)}[k](\mathbf{s}_i^{(n)}[k], a)$  according to (2) for the pendulum to swing to its new state  $\mathbf{s}_{i+1}^{(n)}[k]$  via the earlier met transition module function  $F_{\text{trans}}(\cdot)$ . Noise is *not* considered in the implementation of  $F_{\text{trans}}(\cdot)$ , unlike the case of training data generation. The reason is that the current estimate  $Q^{(n)}[k]$ , despite the fact that it was learned from noisy training data, needs to be validated on noiseless, actual, or ground-truth data. Eventually, the quality of  $Q^{(n)}[k]$



(a) Episodic loss (26)



(b) Distance (27) for different values of  $J_C$  in Algorithm 1



(c) Consensus loss (28)

**Fig. 3:** Network of pendulums (Section IV-A). D-FQ [24]:  $\square$ , D-LSTD [18]:  $\dagger$ , Gossip-NN [25] (NN with 506 parameters):  $\diamond$ , Gossip-NN [25] (NN with 938 parameters):  $\times$ , D-TD[ADMM]:  $\diamond$ , Algorithm 1 ( $D, J_C$ ) = (500, 50):  $\circ$ , Algorithm 1 ( $D, J_C$ ) = (500, 25):  $\star$ , Algorithm 1 ( $D, J_C$ ) = (500, 10):  $-$ , Algorithm 1 ( $D, J_C$ ) = (300, 50):  $\triangle$ . The shaded areas in Figure 3(a) correspond to values in the range of (mean)  $\pm 0.5 \times$  (standard deviation).

is validated by the following “episodic loss”

$$\mathcal{L}_e[k] := \frac{1}{N N_e} \sum_{n \in \mathcal{N}} \sum_{i=0}^{N_e-1} g(\mathbf{s}_i^{(n)}[k], \mathbf{a}_i^{(n)}[k]). \quad (26)$$

For the current scenario,  $N_e = 200$ .



Algorithm 1 is also validated via the normalized distance

$$D_{Q_*}[k] := \frac{1}{N} \sum_{n \in \mathcal{N}} \frac{\|Q^{(n)}[k] - Q_*\|^2}{\|Q_*\|^2} \quad (27)$$

to a fixed point  $Q_*$  of the star-topology map  $T_*$  defined in (6). However, in general,  $Q_*$  cannot be obtained in closed form from (6). Assuming that  $T_*$  is a contraction mapping,  $Q_*$  is taken to be the limit point of the Banach-Picard iteration [36]: for an arbitrarily fixed  $Q_0$ ,  $Q_{k+1} := T_*(Q_k)$ ,  $\forall k \in \mathbb{N}$ .

To assess whether consensus is achieved by the employed algorithms, the following “consensus loss” is considered:

$$\mathcal{L}_c[kM + m] := \frac{1}{N(N-1)} \sum_{n \neq n'} \|Q_m^{(n)}[k] - Q_m^{(n')}[k]\|, \quad (28)$$

where  $k \in \mathbb{N}$  and  $m \in \{0, \dots, M-1\}$ . However, for Gossip-NN [25], where dense NNs are used, the following consensus loss is adopted:

$$\begin{aligned} \mathcal{L}_c^{\text{NN}}[kM + m] &:= \frac{1}{N(N-1)} \sum_{n \neq n'} \left( \sum_{i=1}^{L_{\text{NN}}} \|\mathbf{W}_i^{(n)} - \mathbf{W}_i^{(n')}\|_{\text{F}}^2 \right. \\ &\quad \left. + \|\mathbf{b}_i^{(n)} - \mathbf{b}_i^{(n')}\|^2 \right)^{1/2}, \quad (29) \end{aligned}$$

where  $\mathbf{W}_i^{(n)}$  and  $\mathbf{b}_i^{(n)}$  stand for the matrix of weights and vector of offsets of the  $i$ th NN layer at node  $n$ , respectively.

Figure 3(a) shows that Algorithm 1, with  $(D, J_C) = (500, 50)$  and  $(D, J_C) = (300, 50)$ , outperforms all other methods in terms of the episodic loss (26), as these configurations are positioned closest to the left and bottom edges of the figure. However, a trade-off arises. Reducing the RFF dimension  $D$  from 500 to 300 decreases the cumulative communication cost needed for the curve to reach its “steady state,” since fewer parameters are communicated among agents. On the other hand, the value of the steady-state loss is increased, as using fewer parameters reduces the RFF space’s ability to adequately approximate Q-functions.

It is also important to note that D-TD[ADMM], introduced here to solve (4), achieves the same loss-value level as Algorithm 1 with  $(D, J_C) = (500, 50)$ , but at the cost of significantly higher communication (more than double). Recall that in D-TD[ADMM], agents only communicate their Q-function information. Additionally, increasing the number of NN parameters in Gossip-NN “delays” convergence to a steady state, as more parameters are communicated among agents across  $\mathcal{G}$  per VI iteration. However, this increase leads to a slight improvement in the steady-state loss value, due to the enhanced Q-function approximation capacity provided by the larger number of NN parameters.

Figure 3(b) illustrates the effect of the parameter  $J_C$  in Algorithm 1 on the distance loss (27). The curves confirm that as  $J_C$  increases,  $\mathbf{C}_l^{(n)}$  is shared less frequently among neighbors via (20) in the computation of (22b), resulting in a smaller communication cost footprint. However, the robustness of Algorithm 1 to changes in  $J_C$  is noteworthy: the steady-state loss value appears unaffected by these variations.

Although each method employs different values of  $M$  to achieve consensus among agents between VI iterations (see

Figure 1 and Table I), to assess the consensus quality on a common platform,  $M$  is set to 2000 in Figure 3(c). It is evident that Algorithm 1 achieves consensus quickly with low loss values in (28), supported theoretically by Theorem 5(ii). This justifies the choice of  $M = 50$  in Table I, as there is no need to wait for 2000 iterations before progressing to the next VI recursion (see Figure 1).

### B. Network of cartpoles

Similar to the setup in Section IV-A, a cartpole [39], [42] is assigned to each of the 25 agents on the  $5 \times 5$  grid. A cartpole consists of a cart and a pole (Figure 2(b)), with one end of the pole attached to the cart, which moves horizontally, while the other end is free to move. Following [39], [42], the state of the cartpole at node  $n$  is represented by the tuple  $(x^{(n)}, v^{(n)}, \theta^{(n)}, \dot{\theta}^{(n)})$ , where  $x^{(n)}$  is the horizontal position of the cart,  $v^{(n)}$  is the cart’s velocity,  $\theta^{(n)}$  is the angle between the pole’s current direction and its upright position (similar to the pendulum case), and  $\dot{\theta}^{(n)}$  is the angular velocity. The goal of agent  $n$  is to apply a force/action  $a \in \mathcal{A} := \{-10, 10\}$  to the cart, moving it horizontally such that  $-B_x \leq x^{(n)} \leq B_x$  and  $-B_\theta \leq \theta^{(n)} \leq B_\theta$ , for some  $B_x, B_\theta \in \mathbb{R}_{++}$  [39], [42]. The collective objective is for all agents to collaborate by exchanging information with their neighbors to achieve their individual goals with the least possible communication cost.

To amplify separability between actions in the approximating RKHS  $\mathcal{H}$ , the strategy of [8] is followed here and the generic state-action vector at node  $n$  is defined as

$$\mathbf{z}^{(n)} := \begin{cases} [\frac{x^{(n)}}{4}, \frac{v^{(n)}}{4}, \theta^{(n)}, \frac{\dot{\theta}^{(n)}}{4}, 0, 0, 0, 0]^\top, & \text{if } a = -10, \\ [0, 0, 0, 0, \frac{x^{(n)}}{4}, \frac{v^{(n)}}{4}, \theta^{(n)}, \frac{\dot{\theta}^{(n)}}{4}]^\top, & \text{if } a = 10, \end{cases}$$

where scaling by  $1/4$  was introduced to facilitate learning. Moreover, the one-step loss is defined by

$$g(\mathbf{z}^{(n)}) := \begin{cases} 0, & \text{if } |x^{(n)}| > B_x \text{ or } |\theta^{(n)}| > B_\theta, \\ -1, & \text{otherwise.} \end{cases}$$

The data trajectory  $\mathcal{T}^{(n)}$  of Assumption 1(iii), with  $N_{\text{av}}^{(n)} = 100$ , is generated here in a similar way to Section IV-A. In other words, to mimic realistic scenarios when using the transition module  $F_{\text{trans}}(\cdot)$  of [39], [42] to update  $(x_{i+1}^{(n)}, v_{i+1}^{(n)}, \theta_{i+1}^{(n)}, \dot{\theta}_{i+1}^{(n)}) := F_{\text{trans}}(x_i^{(n)} + \epsilon_1, v_i^{(n)} + \epsilon_2, \theta_i^{(n)} + \epsilon_3, \dot{\theta}_i^{(n)} + \epsilon_4, a_i^{(n)} + \epsilon_5)$ , noise  $\epsilon_k$  that follows the Gaussian PDF  $\mathcal{N}(0, \sigma_k^2)$ ,  $k \in \{1, \dots, 5\}$ , is added, with  $\sigma_1^2 = 0.05$ ,  $\sigma_2^2 = 0.5$ ,  $\sigma_3^2 = 0.05$ ,  $\sigma_4^2 = 0.5$ , and  $\sigma_5^2 = 0.05$ . The only twist here is that in the case where  $|x_{i+1}^{(n)}| > B_x$  or  $|\theta_{i+1}^{(n)}| > B_\theta$ , then  $(x_{i+1}^{(n)}, v_{i+1}^{(n)}, \theta_{i+1}^{(n)}, \dot{\theta}_{i+1}^{(n)})$  is redefined as the initial  $(x_0^{(n)}, v_0^{(n)}, \theta_0^{(n)}, \dot{\theta}_0^{(n)})$  which is provided in [39].

In the current scenario,  $N_e = 500$  in (26), the RFF dimension  $D = 250$  in (16) for all employed methods ( $D = 150$  is also tested in Figure 4(a) for Algorithm 1), and  $\sigma = 0.025$  in (23). All other parameters of Algorithm 1 are kept the same as in Section IV-A.

Figure 4 reveals similar observations to those made at the end of Section IV-A. However, D-LSTD seems to perform better in Figure 4(a) compared to Figure 3(a). Additionally, the differences in convergence speed between the curves in Figure 4(b) are less pronounced than those in Figure 3(b).

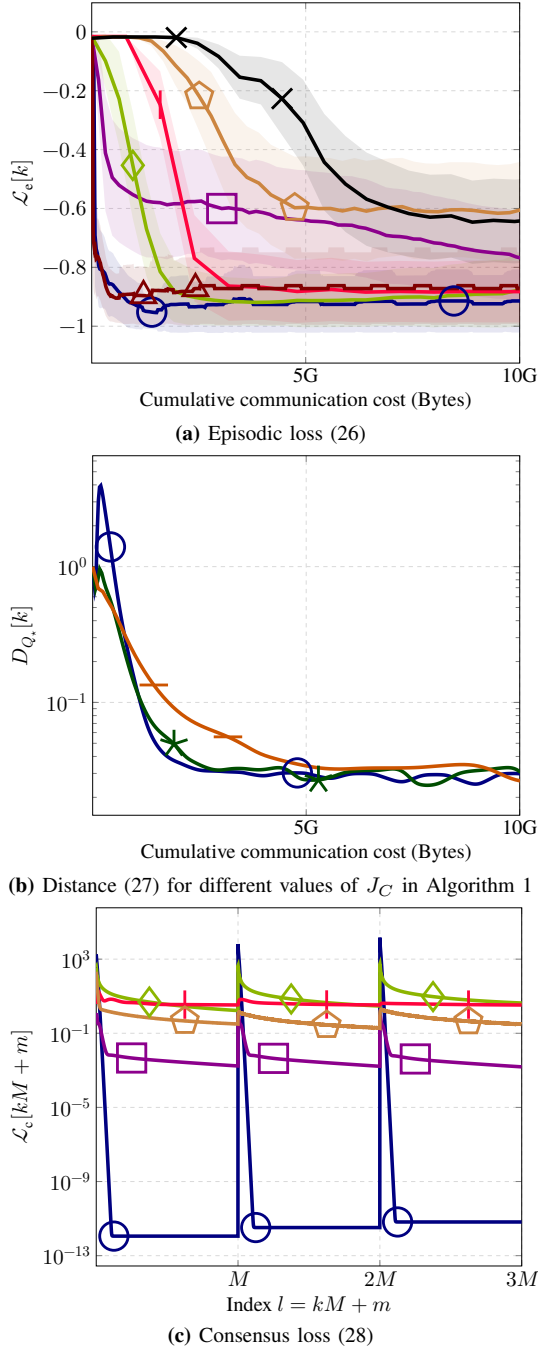


**Fig. 4:** Network of cartpoles (Section IV-B). D-FQ [24]:  $\square$ , D-LSTD [18]:  $\cdot$ , Gossip-NN [25] (NN with 218 parameters):  $\times$ , D-TD[ADMM]:  $\diamond$ , Algorithm 1 ( $D, J_C$ ) = (250, 50):  $\circ$ , Algorithm 1 ( $D, J_C$ ) = (250, 25):  $\star$ , Algorithm 1 ( $D, J_C$ ) = (250, 10):  $-$ , Algorithm 1 ( $D, J_C$ ) = (150, 50):  $\triangle$ . The shaded areas in Figure 4(a) correspond to values in the range of  $(\text{mean}) \pm 0.5 \times (\text{standard deviation})$ .

## V. CONCLUSIONS

A novel class of nonparametric Bellman mappings (B-Maps) was introduced for value iteration (VI) in distributed reinforcement learning (DRL). This approach leveraged a reproducing kernel Hilbert space representation of the Q-function, enabling a nonparametric formulation that supports flexible, agent-specific basis function design. Beyond sharing Q-functions, agents also exchanged basis information without

relying on a centralized fusion center, facilitating consensus. The proposed methodology was backed by rigorous theoretical analysis, and numerical evaluations on two well-known control problems demonstrated its superior performance compared to existing methods. Interestingly, the evaluations revealed a counter-intuitive insight: despite involving increased information exchange—specifically through covariance matrix sharing—the approach achieved the desired performance with lower cumulative communication cost than prior-art DRL schemes. This underscores the critical role of basis information in accelerating the learning process.

Ongoing research aims to extend this framework to on-line/streaming data, integrate state-sharing mechanisms common in a plethora of multi-agent reinforcement learning (MARL) designs, and develop strategies to reduce the computational complexity of the matrix inversion in (23).

## APPENDIX

The discussion starts with the following lemma to establish properties on recursions (15) and (22). To save space, those recursions are unified in the generic form of (30).

**Lemma 7.** For the user-defined  $\mathbf{x}_{-1}, \mathbf{x}' \in \mathbb{R}^N$ , generate sequence  $(\mathbf{x}_m)_{m \in \mathbb{N}} \subset \mathbb{R}^N$  by

$$\mathbf{x}_0 := A_\varpi(\mathbf{x}_{-1}) - \eta(\mathbf{x}_{-1} - N\mathbf{x}') \quad (30a)$$

$$\mathbf{x}_{m+1} := \mathbf{x}_m - (A_\varpi(\mathbf{x}_{m-1}) - \eta\mathbf{x}_{m-1}) + (A(\mathbf{x}_m) - \eta\mathbf{x}_m), \quad \forall m \in \mathbb{N}, \quad (30b)$$

where  $\varpi \in [1/2, 1)$ ,  $\eta \in (0, 2(1 - \varpi))$ ,  $A := \mathbf{I}_N - \gamma\mathbf{L}$ , with  $\mathbf{L}$  being the  $N \times N$  graph Laplacian matrix, and  $A_\varpi := \varpi A + (1 - \varpi)\mathbf{I}_N$ . Then,  $0 < \varrho(\eta) < 1$  (Theorem 5(i)), and

$$\|\mathbf{x}_m - \mathbf{x}_*\| = \mathcal{O}(m\varrho^m(\eta)), \quad (31)$$

where  $\mathbf{x}_* := [\mathbf{1}_N^\top \mathbf{x}', \dots, \mathbf{1}_N^\top \mathbf{x}']^\top = \mathbf{1}_{N \times N} \mathbf{x}' \in \mathbb{R}^N$ .

*Proof:* Notice that (30) can be recast as

$$\mathbf{x}_0 = [\varpi(\mathbf{I}_N - \gamma\mathbf{L}) + (1 - \varpi)\mathbf{I}_N - \eta\mathbf{I}_N]\mathbf{x}_{-1} + \eta N\mathbf{x}', \quad (32a)$$

and

$$\begin{aligned} \mathbf{x}_{m+1} &= \mathbf{x}_m - (\varpi(\mathbf{I}_N - \gamma\mathbf{L})\mathbf{x}_{m-1} + (1 - \varpi)\mathbf{x}_{m-1} - \eta\mathbf{x}_{m-1}) \\ &\quad + ((\mathbf{I}_N - \gamma\mathbf{L})\mathbf{x}_m - \eta\mathbf{x}_m) \\ &= ((2 - \eta)\mathbf{I}_N - \gamma\mathbf{L})\mathbf{x}_m + (\varpi\gamma\mathbf{L} + (\eta - 1)\mathbf{I}_N)\mathbf{x}_{m-1}. \end{aligned} \quad (32b)$$

Define  $\mathbf{a}_m := \mathbf{U}^\top \mathbf{x}_m$  and  $\mathbf{a}' := \mathbf{U}^\top \mathbf{x}'$ , where  $\mathbf{U}$  is obtained by the EVD of  $\mathbf{L}$ , and let  $a_m^{(n)}$  and  $a'^{(n)}$  be the  $n$ th entries of  $\mathbf{a}_m$  and  $\mathbf{a}'$ , respectively. Applying  $\mathbf{U}^\top$  to (32) yields that  $\forall n \in \mathcal{N} := \{1, \dots, N\}$ ,

$$a_0^{(n)} = -q_n a_{-1}^{(n)} + \eta N a'^{(n)}, \quad (33a)$$

and  $\forall m \in \mathbb{N}$ ,

$$\begin{aligned} a_{m+1}^{(n)} &= (2 - \eta - \gamma\lambda_n) a_m^{(n)} + (\varpi\gamma\lambda_n + \eta - 1) a_{m-1}^{(n)} \\ &= p_n a_m^{(n)} + q_n a_{m-1}^{(n)}. \end{aligned} \quad (33b)$$

Let

$$\theta_n^+ := \frac{p_n + \sqrt{p_n^2 + 4q_n}}{2}, \quad \theta_n^- := \frac{p_n - \sqrt{p_n^2 + 4q_n}}{2},$$

be the solutions of the quadratic equation  $\theta^2 - p_n\theta - q_n = 0$ , so that  $p_n = \theta_n^+ + \theta_n^-$  and  $q_n = -\theta_n^+\theta_n^-$ . As such, (33b) yields

$$\begin{aligned} a_{m+1}^{(n)} - \theta_n^+ a_m^{(n)} &= \theta_n^- \overbrace{(a_m^{(n)} - \theta_n^+ a_{m-1}^{(n)})}^{\Delta_m^{(n)+}}, \\ a_{m+1}^{(n)} - \theta_n^- a_m^{(n)} &= \theta_n^+ \overbrace{(a_m^{(n)} - \theta_n^- a_{m-1}^{(n)})}^{\Delta_m^{(n)-}}, \end{aligned} \quad (34)$$

which lead by induction to the following:  $\forall m \in \mathbb{N}_*, \forall n \in \mathcal{N}$ ,

$$\Delta_m^{(n)+} = (\theta_n^-)^m \Delta_0^{(n)+}, \quad (35a)$$

$$\Delta_m^{(n)-} = (\theta_n^+)^m \Delta_0^{(n)-}, \quad (35b)$$

with

$$\Delta_0^{(n)+} = -(q_n + \theta_n^+)a_{-1}^{(n)} + \eta N a'^{(n)}, \quad (35c)$$

$$\Delta_0^{(n)-} = -(q_n + \theta_n^-)a_{-1}^{(n)} + \eta N a'^{(n)}. \quad (35d)$$

The case of  $n \in \mathcal{N} \setminus \{N\}$  will be now considered. Recall that in this case  $\lambda_n > 0$ . First, does there exist an  $n \in \mathcal{N} \setminus \{N\}$  s.t.  $\theta_n^+ = 1$ ? The answer is negative. To see this, assume for a contradiction that  $\theta_n^+ = 1$  for some  $n \in \mathcal{N} \setminus \{N\}$ . Then, because  $p_n = \theta_n^+ + \theta_n^-$ ,

$$\begin{aligned} p_n &= 1 + \theta_n^- \\ \Rightarrow 2 - 2\eta - 2\gamma\lambda_n &= 2\theta_n^- = p_n - \sqrt{p_n^2 + 4q_n} \\ \Rightarrow \eta + \gamma\lambda_n &= \sqrt{p_n^2 + 4q_n} \\ \Rightarrow (\eta + \gamma\lambda_n)^2 &= 4 + (\eta + \gamma\lambda_n)^2 - 4(\eta + \gamma\lambda_n) + 4q_n \\ \Rightarrow \gamma\lambda_n &= \varpi\gamma\lambda_n \quad (\gamma\lambda_n \neq 0) \\ \Rightarrow 1 &= \varpi, \end{aligned}$$

which contradicts the original design  $\varpi < 1$ .

It has been already noted by the discussion after (15) that sequence  $(\mathbf{x}_m)_{m \in \mathbb{N}}$  converges. Hence,  $(\mathbf{a}_m = \mathbf{U}^\top \mathbf{x}_m)_{m \in \mathbb{N}}$  converges  $\Rightarrow (\Delta_m^{(n)-})_{m \in \mathbb{N}}$  converges  $\Rightarrow (\Delta_m^{(n)-})_{m \in \mathbb{N}}$  is a Cauchy sequence  $\Rightarrow |\Delta_{m+1}^{(n)-} - \Delta_m^{(n)-}|$  converges to zero. Because  $\mathbf{x}_{-1}$  can be arbitrarily fixed, it can be chosen so that  $\Delta_0^{(n)-} \neq 0, \forall n \in \mathcal{N} \setminus \{N\}$ ; see (35d). Notice now that  $|\Delta_{m+1}^{(n)-} - \Delta_m^{(n)-}| = |\theta_n^+|^m |\theta_n^+ - 1| |\Delta_0^{(n)-}|$ , which suggests that  $\forall n \in \mathcal{N} \setminus \{N\}, |\theta_n^+|^m = |\Delta_{m+1}^{(n)-} - \Delta_m^{(n)-}| / (|\theta_n^+ - 1| |\Delta_0^{(n)-}|)$  converges to zero, and this is feasible only if  $|\theta_n^+| < 1$ . Observe also that  $1 - \eta < 1$  to establish  $0 < \varrho(\eta) < 1$  (Theorem 5(i)).

Consider the case where  $n \in \mathcal{N} \setminus \{N\}$  and  $p_n^2 + 4q_n \neq 0$ . Then,  $\theta_n^- \neq \theta_n^+$ . Moreover, because  $p_n = 2 - \eta - \gamma\lambda_n \geq 2 - 2(1 - \varpi) - 1 \geq 2 - 1 - 1 = 0$ , it can be verified that  $|\theta_n^-| \leq |\theta_n^+|$ . Multiplying (35a) by  $\theta_n^-$  and (35b) by  $\theta_n^+$  and subtracting the resultant equations yield

$$\begin{aligned} |a_m^{(n)}| &= \frac{1}{|\theta_n^+ - \theta_n^-|} |(\theta_n^+)^{m+1} \Delta_0^{(n)-} - (\theta_n^-)^{m+1} \Delta_0^{(n)+}| \\ &= \frac{1}{|\theta_n^+ - \theta_n^-|} |(\theta_n^+)^{m+1} \Delta_0^{(n)-} - (\theta_n^-)^{m+1} \Delta_0^{(n)-}| \end{aligned}$$

$$\begin{aligned} &+ (\theta_n^-)^{m+1} \Delta_0^{(n)-} - (\theta_n^-)^{m+1} \Delta_0^{(n)+}| \\ &\leq \frac{|(\theta_n^+)^{m+1} - (\theta_n^-)^{m+1}|}{|\theta_n^+ - \theta_n^-|} |\Delta_0^{(n)-}| \\ &\quad + |(\theta_n^-)|^{m+1} \frac{|\Delta_0^{(n)-} - \Delta_0^{(n)+}|}{|\theta_n^+ - \theta_n^-|} \\ &= \left| \sum_{k=0}^m (\theta_n^+)^{m-k} (\theta_n^-)^k \right| |\Delta_0^{(n)-}| \\ &\quad + |(\theta_n^-)|^{m+1} \frac{|a_{-1}^{(n)} (\theta_n^+ - \theta_n^-)|}{|\theta_n^+ - \theta_n^-|} \\ &\leq (m+1) |(\theta_n^+)|^m |\Delta_0^{(n)-}| + |(\theta_n^-)|^m |a_{-1}^{(n)}| \\ &\leq 2m |(\theta_n^+)|^m |\Delta_0^{(n)-}| + m |(\theta_n^+)|^m |a_{-1}^{(n)}| \\ &\leq C_n m \varrho^m(\eta) \leq C m \varrho^m(\eta), \end{aligned}$$

for some  $C_n \in \mathbb{R}_{++}$  and  $C := \max_{n \in \mathcal{N} \setminus \{N\}} C_n$ . It is worth stressing here that  $C_n$  and  $C$  depend on  $\mathbf{a}_{-1}$ ,  $\mathbf{a}'$ , and hence on  $\mathbf{x}_{-1}$  and  $\mathbf{x}'$ . This delicate point will be addressed at (37) via Assumption 4(iv).

Consider now the case where  $n \in \mathcal{N} \setminus \{N\}$  with  $p_n^2 + 4q_n = 0$ . Then,  $\theta_n^+ = \theta_n^- = p_n/2$ , and induction on (35a), together with (33a), yield

$$\begin{aligned} a_m^{(n)} &= \left(\frac{p_n}{2}\right)^m a_0^{(n)} + m \left(\frac{p_n}{2}\right)^m \Delta_0^{(n)+} \\ &= \left(\frac{p_n}{2}\right)^m \left[ \left(\frac{p_n}{2}\right)^2 a_{-1}^{(n)} + \eta N a'^{(n)} \right] \\ &\quad + m \left(\frac{p_n}{2}\right)^m \left[ \left(\frac{p_n}{2}\right) \left(\frac{p_n}{2} - 1\right) a_{-1}^{(n)} + \eta N a'^{(n)} \right]. \end{aligned}$$

Because  $|p_n/2| \leq \varrho(\eta)$ , the previous result suggests that there exists  $C_n \in \mathbb{R}_{++}$  s.t.  $|a_m^{(n)}| \leq C_n m \varrho^m(\eta)$ .

Consider now the case of  $n = N$ . Recall that  $\lambda_N = 0$  and the  $N$ th column of  $\mathbf{U}$  is  $\mathbf{1}_N / \sqrt{N}$ . Then,  $p_N = 2 - \eta$ ,  $q_N = \eta - 1$ ,  $p_N^2 + 4q_N = \eta^2$ ,  $\theta_N^+ = 1$ , and  $\theta_N^- = 1 - \eta$ . Notice also that the  $N$ th entry of vector  $\mathbf{a}'$  is  $a'^{(N)} = (1/\sqrt{N}) \mathbf{1}_N^\top \mathbf{x}'$ . Now, adding (33a) to copies of (34) for consecutive values of  $m$  yields

$$\begin{aligned} a_m^{(N)} &= (1 - \eta) a_{-1}^{(N)} + \eta N a'^{(N)} + (1 - \eta) \sum_{k=0}^{m-1} \Delta_k^{(N)+} \\ &= (1 - \eta) a_{-1}^{(N)} + \eta N a'^{(N)} + (1 - \eta) \sum_{k=0}^{m-1} (1 - \eta)^k \Delta_0^{(N)+} \\ &= N a'^{(N)} + (1 - \eta)^{m+1} (a_{-1}^{(N)} - N a'^{(N)}) \\ &= \sqrt{N} \mathbf{1}_N^\top \mathbf{x}' + (1 - \eta)^{m+1} (a_{-1}^{(N)} - \sqrt{N} \mathbf{1}_N^\top \mathbf{x}'). \end{aligned}$$

Therefore, there exists  $C_N \in \mathbb{R}_{++}$  s.t.

$$\begin{aligned} |a_m^{(N)} - \sqrt{N} \mathbf{1}_N^\top \mathbf{x}'| &= (1 - \eta)^{m+1} |a_{-1}^{(N)} - \sqrt{N} \mathbf{1}_N^\top \mathbf{x}'| \\ &\leq (1 - \eta)^{m+1} (|a_{-1}^{(N)}| + N \|\mathbf{x}'\|) \\ &\leq C_N (1 - \eta)^{m+1} \leq C_N (1 - \eta)^m \\ &\leq C_N \varrho^m(\eta) \leq C_N m \varrho^m(\eta). \end{aligned}$$

To summarize all of the previous findings, recall that  $\mathbf{1}_N/\sqrt{N}$  is the  $N$ th column of the orthogonal  $\mathbf{U}$ , so that  $\mathbf{U}^\top \mathbf{1}_N = [0, 0, \dots, \sqrt{N}]^\top$ , and

$$\begin{aligned} \mathbf{a}_* &:= \mathbf{U}^\top \mathbf{x}_* = \mathbf{U}^\top [\mathbf{1}_N, \dots, \mathbf{1}_N] \mathbf{x}' \\ &= \begin{bmatrix} \mathbf{0}^\top \\ \vdots \\ \mathbf{0}^\top \\ \sqrt{N} \mathbf{1}_N^\top \end{bmatrix} \mathbf{x}' = \begin{bmatrix} 0 \\ \vdots \\ 0 \\ \sqrt{N} \mathbf{1}_N^\top \mathbf{x}' \end{bmatrix}. \end{aligned}$$

Therefore, there exists  $C \in \mathbb{R}_{++}$  s.t.

$$\begin{aligned} \|\mathbf{x}_m - \mathbf{x}_*\|^2 &= \|\mathbf{U}(\mathbf{x}_m - \mathbf{x}_*)\|^2 = \|\mathbf{a}_m - \mathbf{a}_*\|^2 \\ &= \sum_{n \in \mathcal{N} \setminus \{N\}} |a_m^{(n)}|^2 + |a_m^{(N)} - \sqrt{N} \mathbf{1}_N^\top \mathbf{x}'|^2 \\ &\leq C m^2 \varrho^{2m}(\eta), \end{aligned}$$

which establishes (31).  $\blacksquare$

Now, by applying the transpose operator  $\top$  to (15) and by recalling that  $\mathbf{L}$  is symmetric, it can be verified that (15) can be viewed as (30), where  $\mathbf{x}_m$  refers to the  $d$ th column  $\mathbf{q}_m^{(d)}[k]$  ( $d \in \{1, \dots, D\}$ ) of the  $N \times D$  matrix  $\mathbf{\Omega}_m^\top[k]$ ,  $\mathbf{x}_{-1}$  refers to the  $d$ th column of  $\mathbf{\Omega}_{-1}^\top[k]$ ,  $\mathbf{x}'$  to the  $d$ th column  $\mathbf{q}_T^{(d)}[k]$  of  $\mathbf{T}^\top(\mathbf{\Omega}[k])$ ,  $\mathbf{x}_* = \mathbf{1}_{N \times N} \mathbf{q}_T^{(d)}[k]$ , and  $A := A^\mathbf{Q}$ . Then, by stacking together all of the aforementioned  $D$  columns into matrices and by applying Lemma 7, it can be verified that there exists  $C \in \mathbb{R}_{++}$  s.t.

$$\begin{aligned} C m^2 \varrho^{2m}(\eta) &\geq \sum_{d \in \{1, \dots, D\}} \|\mathbf{q}_m^{(d)}[k] - \mathbf{1}_{N \times N} \mathbf{q}_T^{(d)}[k]\|^2 \\ &= \|\mathbf{\Omega}_m^\top[k] - \mathbf{1}_{N \times N} [\mathbf{q}_T^{(1)}[k], \dots, \mathbf{q}_T^{(D)}[k]]\|_F^2 \\ &= \|\mathbf{\Omega}_m^\top[k] - \mathbf{1}_{N \times N} \mathbf{T}^\top(\mathbf{\Omega}[k])\|_F^2 \\ &= \|\mathbf{\Omega}_m[k] - \mathbf{T}(\mathbf{\Omega}[k]) \mathbf{1}_{N \times N}\|_F^2 \\ &= \sum_{n \in \mathcal{N}} \|Q_m^{(n)}[k] - \mathbf{T}(\mathbf{\Omega}[k]) \mathbf{1}_N\|^2 \\ &\geq \|Q_m^{(n)}[k] - \mathbf{T}(\mathbf{\Omega}[k]) \mathbf{1}_N\|^2, \end{aligned}$$

which establishes Theorem 5(ii). A similar sequence of arguments leads to the proof of Theorem 5(iii).

To prove Theorem 5(iv), notice first that

$$\begin{aligned} &\|Q^{(n)}[k+1] - Q_*\| \\ &= \|Q_M^{(n)}[k] - Q_*\| \\ &\leq \|T_*(Q^{(n)}[k]) - Q_*\| + \|\mathbf{T}(\mathbf{\Omega}[k]) \mathbf{1}_N - T_*(Q^{(n)}[k])\| \\ &\quad + \|Q_M^{(n)}[k] - \mathbf{T}(\mathbf{\Omega}[k]) \mathbf{1}_N\| \\ &\leq \beta_* \|Q^{(n)}[k] - Q_*\| + \|\mathbf{T}(\mathbf{\Omega}[k]) \mathbf{1}_N - T_*(Q^{(n)}[k])\| \\ &\quad + \|Q_M^{(n)}[k] - \mathbf{T}(\mathbf{\Omega}[k]) \mathbf{1}_N\|, \end{aligned} \quad (36)$$

where the second inequality holds because of Assumption 4(ii). Observe now that

$$\begin{aligned} &T_*(Q^{(n)}[k]) \\ &= \sum_{n' \in \mathcal{N}} \Psi_*^{(n')} \mathbf{c}^{(n')}(Q^{(n)}[k]) \\ &= \sum_{n' \in \mathcal{N}} \Psi^{(n')}[k] \mathbf{c}^{(n')}(Q^{(n)}[k]) \\ &\quad + \sum_{n' \in \mathcal{N}} (\Psi_*^{(n')} - \Psi^{(n')}[k]) \mathbf{c}^{(n')}(Q^{(n)}[k]) \\ &= \sum_{n' \in \mathcal{N}} T^{(n')}(Q^{(n)}[k]) \end{aligned}$$

$$+ \sum_{n' \in \mathcal{N}} (\Psi_*^{(n')} - \Psi^{(n')}[k]) \mathbf{c}^{(n')}(Q^{(n)}[k]).$$

An inspection of (7b) and (23), under the light of Theorem 5(iii), and the continuity of the mapping  $(\cdot + \sigma \mathbf{I}_D)^{-1}$  suggest that for an arbitrarily fixed  $\epsilon \in \mathbb{R}_{++}$  and for all sufficiently large  $k$ ,  $\|\Psi_*^{(n')} - \Psi^{(n')}[k]\|_F \leq \epsilon$ . Further, by Assumption 4(iv), there exists a  $C'' \in \mathbb{R}_{++}$  such that for all sufficiently large  $k$ ,

$$\sum_{n' \in \mathcal{N}} \|(\Psi_*^{(n')} - \Psi^{(n')}[k]) \mathbf{c}^{(n')}(Q^{(n)}[k])\| \leq C'' \epsilon.$$

Via the previous observations,

$$\begin{aligned} &\|\mathbf{T}(\mathbf{\Omega}[k]) \mathbf{1}_N - T_*(Q^{(n)}[k])\| \\ &\leq \|\sum_{n' \in \mathcal{N}} T^{(n')}(Q^{(n')}[k]) - \sum_{n' \in \mathcal{N}} T^{(n')}(Q^{(n)}[k])\| \\ &\quad + \sum_{n' \in \mathcal{N}} \|(\Psi_*^{(n')} - \Psi^{(n')}[k]) \mathbf{c}^{(n')}(Q^{(n)}[k])\| \\ &\leq \sum_{n' \in \mathcal{N}} \|T^{(n')}(Q^{(n')}[k]) - T^{(n')}(Q^{(n)}[k])\| + C'' \epsilon \\ &\leq \sum_{n' \in \mathcal{N}} \beta^{(n')}[k] \|Q^{(n')}[k] - Q^{(n)}[k]\| + C'' \epsilon \\ &\leq \sum_{n' \in \mathcal{N}} \beta^{(n')}[k] \|Q^{(n')}[k] - \mathbf{T}(\mathbf{\Omega}[k-1]) \mathbf{1}_N\| \\ &\quad + \sum_{n' \in \mathcal{N}} \beta^{(n')}[k] \|\mathbf{T}(\mathbf{\Omega}[k-1]) \mathbf{1}_N - Q^{(n)}[k]\| + C'' \epsilon \\ &\leq C' \sum_{n' \in \mathcal{N}} \|Q_M^{(n')}[k-1] - \mathbf{T}(\mathbf{\Omega}[k-1]) \mathbf{1}_N\| \\ &\quad + NC' \|\mathbf{T}(\mathbf{\Omega}[k-1]) \mathbf{1}_N - Q_M^{(n)}[k-1]\| + C'' \epsilon, \end{aligned}$$

where Assumption 4(iii) on  $\beta^{(n')}[k]$  was also utilized. Therefore, (36) becomes

$$\begin{aligned} &\|Q^{(n)}[k+1] - Q_*\| \\ &\leq \beta_* \|Q^{(n)}[k] - Q_*\| \\ &\quad + C' \sum_{n' \in \mathcal{N}} \|Q_M^{(n')}[k-1] - \mathbf{T}(\mathbf{\Omega}[k-1]) \mathbf{1}_N\| \\ &\quad + NC' \|\mathbf{T}(\mathbf{\Omega}[k-1]) \mathbf{1}_N - Q_M^{(n)}[k-1]\| + C'' \epsilon \\ &\quad + \|Q_M^{(n)}[k] - \mathbf{T}(\mathbf{\Omega}[k]) \mathbf{1}_N\| \\ &\leq \beta_* \|Q^{(n)}[k] - Q_*\| + C(M \varrho^M(\eta) + \epsilon), \end{aligned} \quad (37)$$

for some  $C \in \mathbb{R}_{++}$ , where the existence of  $C$  is ensured by  $C''$ , Theorem 5(ii) and Assumption 4(iv). Now, by using induction on (37), it can be verified that there exists a sufficiently large  $k_0 \in \mathbb{N}_*$  such that for all  $\mathbb{N}_* \ni k > k_0$ ,

$$\begin{aligned} &\|Q^{(n)}[k+k_0] - Q_*\| \leq \beta_*^k \|Q^{(n)}[k_0] - Q_*\| \\ &\quad + C(M \varrho^M(\eta) + \epsilon) \sum_{i=0}^{k-1} \beta_*^i. \end{aligned}$$

The application of  $\limsup_{k \rightarrow \infty}$  to both sides of the previous inequality and the fact that  $\epsilon \in \mathbb{R}_{++}$  was arbitrarily fixed establish Theorem 5(iv).

Moving on to the proof of Theorem 6, notice that under Assumptions 4(i) and 4(v),  $p_n + (p_n^2 + 4q_n)^{1/2} = 2 - \eta - b_n + (b_n^2 + 2(\eta - 1)b_n + \eta^2)^{1/2}$  in (25a).

**Lemma 8.** Let  $\eta \in (0, 1)$  and  $b_{N-1} \in (0, 1/2)$ . Define the continuous function  $f_\eta: (0, 1] \rightarrow \mathbb{R}: b \mapsto f_\eta(b) := |d_\eta(b)|^2$ , where

$$d_\eta(b) := 2 - \eta - b + \sqrt{b^2 + 2(\eta - 1)b + \eta^2}.$$

Then,  $\forall \eta \in (0, 1)$ ,  $b_{N-1} \in \arg \max_{\{b_n \mid n \in \mathcal{N} \setminus \{N\}\}} f_\eta(b_n)$ .

*Proof:* Notice that  $\forall b \in (0, 1]$ ,  $2 - \eta - b > 2 - 1 - 1 = 0$ . Consider first the case  $\eta > 1/2$ . Then  $\forall b \in (0, 1]$ ,  $b^2 + 2(\eta - 1)b + \eta^2 > b^2 - b + 1/4 = (b - 1/2)^2 \geq 0 \Rightarrow d_\eta(b) > 0 \Rightarrow f_\eta(b) = d_\eta^2(b) \Rightarrow$

$$f'_\eta(b) = 2d_\eta(b) \left( -1 + \frac{b + \eta - 1}{\sqrt{b^2 + 2(\eta - 1)b + \eta^2}} \right). \quad (38)$$

Now, by

$$b^2 + 2(\eta - 1)b + \eta^2 = (b + \eta - 1)^2 + 2\eta - 1, \quad (39)$$

and  $\eta > 1/2$ , it can be verified that  $f'_\eta(b) < 0$  in (38). Hence  $f_\eta(\cdot)$  is monotonically decreasing on  $(0, 1]$ , and for any  $n \in \mathcal{N} \setminus \{N\}$ ,  $f_\eta(b_{N-1}) \geq f_\eta(b_n)$  because  $b_{N-1} \leq b_{N-2} \leq \dots \leq b_1 = 1$ .

The following refer to the case  $\eta \leq 1/2$ . Define  $x_1 := 1 - \eta - \sqrt{1 - 2\eta} > 0$  and  $x_2 := 1 - \eta + \sqrt{1 - 2\eta}$ , and notice that  $x_1 < 1$  and  $x_2 < 2(1 - \eta) < 2 - \eta$ . Use (39) to verify that if  $b \in (0, x_1) \Rightarrow b^2 + 2(\eta - 1)b + \eta^2 > 0 \Rightarrow d_\eta(b) > 2 - \eta - b \geq 2 - 1/2 - b = 3/2 - b > 1/2 > 0 \Rightarrow f'_\eta(b)$  is given by (38). Moreover,  $b + \eta - 1 < x_1 + \eta - 1 \leq 0 \Rightarrow f'_\eta(b) < 0$ . Hence,  $f_\eta(\cdot)$  is monotonically decreasing on  $(0, x_1)$ , and  $f_\eta(b_{N-1}) \geq \max\{f_\eta(b_n) \mid b_n \in (0, x_1), n \in \mathcal{N} \setminus \{N\}\}$  whenever the latter set is nonempty.

If  $b \in [x_1, x_2] \cap (0, 1]$ , then by (39),  $b^2 + 2(\eta - 1)b + \eta^2 \leq 0 \Rightarrow f_\eta(b) = (2 - \eta - b)^2 - (b^2 + 2(\eta - 1)b + \eta^2) = -2b + 4 - 4\eta$ . Thus  $f_\eta(\cdot)$  is monotonically decreasing on  $[x_1, x_2]$ , and  $f_\eta(b_{N-1}) \geq \max\{f_\eta(b_n) \mid b_n \in [x_1, x_2], n \in \mathcal{N} \setminus \{N\}\}$ . Notice also that  $b_{N-1} < 1/2 \leq 1 - \eta \leq x_2 \Rightarrow f_\eta(b_{N-1}) \geq f_\eta(1/2)$ . These results hold true even if  $x_2 \geq 1$ .

Consider finally the case  $x_2 < 1$ . Extend function  $f_\eta$  to the continuous  $\bar{f}_\eta: (x_2, +\infty) \rightarrow \mathbb{R}: b \mapsto \bar{f}_\eta(b) := |d_\eta(b)|^2$ , so that  $\bar{f}_\eta|_{(x_2, 1]} = f_\eta$ . Notice that  $\forall b > x_2$ , by (39) and  $b + \eta - 1 > x_2 + \eta - 1 = (1 - 2\eta)^{1/2} \geq 0 \Rightarrow b^2 + 2(\eta - 1)b + \eta^2 > (x_2 + \eta - 1)^2 + 2\eta - 1 = 1 - 2\eta + 2\eta - 1 = 0 \Rightarrow (b + \eta - 1)/(b^2 + 2(\eta - 1)b + \eta^2)^{1/2} \geq 1$  and  $\bar{f}_\eta(b) = d_\eta^2(b)$ .

The monotonicity of  $\bar{f}_\eta(b)$  on  $(x_2, +\infty)$  is going to be explored next. The case where  $b \in (x_2, 2 - \eta]$  is considered first:  $b \leq 2 - \eta \Rightarrow 2 - \eta - b \geq 0 \Rightarrow d_\eta(b) > 0 \Rightarrow \bar{f}'_\eta(b) \geq 0$ . In the case where  $b > 2 - \eta$ , notice from  $4 - 4\eta - 2b < 4 - 4\eta - 2(2 - \eta) = -2\eta < 0$  and  $2 - \eta - b < 0$  that

$$\begin{aligned} d_\eta(b) &= \frac{(2 - \eta - b)^2 - (b^2 + 2(\eta - 1)b + \eta^2)}{2 - \eta - b - \sqrt{b^2 + 2(\eta - 1)b + \eta^2}} \\ &= \frac{4 - 4\eta - 2b}{2 - \eta - b - \sqrt{b^2 + 2(\eta - 1)b + \eta^2}} > 0. \end{aligned}$$

Hence,  $\bar{f}'_\eta(b) \geq 0$ . To summarize,  $\bar{f}_\eta(\cdot)$  is monotonically non-decreasing on  $(x_2, +\infty)$ . Thus,  $\forall b \in (x_2, +\infty)$ ,  $\bar{f}_\eta(b) \leq \lim_{b' \rightarrow \infty} \bar{f}_\eta(b') = \lim_{b' \rightarrow \infty} d_\eta^2(b') = 1$ . It has been already noted earlier that  $f_\eta(b_{N-1}) \geq f_\eta(1/2)$ . Consequently,  $\forall b \in (x_2, 1]$  and for  $\eta \leq 1/2$ ,  $f_\eta(b_{N-1}) \geq f_\eta(1/2) = d_\eta^2(1/2) \geq (3/2 - \eta)^2 \geq 1 \geq \bar{f}_\eta(b) = f_\eta(b)$ . This establishes  $f_\eta(b_{N-1}) \geq \max\{f_\eta(b_n) \mid b_n \in (x_2, 1], n \in \mathcal{N} \setminus \{N\}\}$  whenever the latter set is nonempty. ■

**Lemma 9.** For  $b \in (0, 1/2)$ , define  $h_b: (0, 1) \rightarrow \mathbb{R}: \eta \mapsto h_b(\eta)$  as

$$h_b(\eta) := \frac{|2 - \eta - b + \sqrt{\eta^2 + 2(\eta - 1)b + b^2}|^2}{4}.$$

Then,  $-b + \sqrt{2b} = \arg \min_{\eta \in (0, 1)} h_b(\eta)$ .

*Proof:* Notice that  $\eta \in (0, -b + (2b)^{1/2}] \Rightarrow \eta^2 + 2(\eta - 1)b + b^2 \leq 0 \Rightarrow h_b(\eta) = (1/4)((2 - \eta - b)^2 - (\eta^2 + 2b\eta + b^2 - 2b)) = (1/2)(-2\eta + 2 - b) \Rightarrow h'_b(\eta) = -1 < 0$ ,  $\forall \eta \in (0, -b + (2b)^{1/2}]$ .

Next,  $\eta \in (-b + (2b)^{1/2}, 1) \Rightarrow \eta^2 + 2b\eta + b^2 - 2b > 0$ , and

$$\begin{aligned} h'_b(\eta) &= \frac{2 - \eta - b + \sqrt{\eta^2 + 2b\eta + b^2 - 2b}}{2} \\ &\quad \cdot \left( -1 + \frac{\eta + b}{\sqrt{\eta^2 + 2b\eta + b^2 - 2b}} \right). \end{aligned}$$

Because  $\eta + b > 0$  and  $\eta^2 + 2b\eta + b^2 - 2b < (\eta + b)^2$ ,  $(\eta + b)/(\eta^2 + 2b\eta + b^2 - 2b)^{1/2} > 1$ . Moreover,  $2 - \eta - b + (\eta^2 + 2b\eta + b^2 - 2b)^{1/2} > 0 \Rightarrow h'_b(\eta) > 0$ ,  $\forall \eta \in (-b + (2b)^{1/2}, 1)$ . Therefore, the claim of Lemma 9 holds true. ■

By Lemma 9, define  $\eta_* := -b_{N-1} + (2b_{N-1})^{1/2}$ , and notice that  $\forall \eta \in (0, 1)$ ,  $|1 - (2b_{N-1})^{1/2}/2| = h_{b_{N-1}}^{1/2}(\eta_*) \leq h_{b_{N-1}}^{1/2}(\eta)$ . Moreover, by  $b_{N-1} \in (0, 1/2)$ , then  $(2b_{N-1})^{1/2}/2 \leq -b_{N-1} + (2b_{N-1})^{1/2} \leq 1$ , and

$$\begin{aligned} h_{b_{N-1}}^{1/2}(\eta_*) &= |1 - (2b_{N-1})^{1/2}/2| \\ &\geq |1 - (-b_{N-1} + (2b_{N-1})^{1/2})| \\ &= |1 - \eta_*| = 1 - \eta_*. \end{aligned} \quad (40)$$

Observe now by the definitions of  $f_\eta, h_b$  in Lemmata 8 and 9 that  $\forall \eta \in (0, 1)$ ,  $\forall b \in (0, 1)$ ,  $h_b(\eta) = f_\eta(b)/4$  and

$$\begin{aligned} \arg \max_{b_n \mid n \in \mathcal{N} \setminus \{N\}} h_{b_n}^{1/2}(\eta) \\ = \arg \max_{b_n \mid n \in \mathcal{N} \setminus \{N\}} f_\eta^{1/2}(b_n) \ni b_{N-1}. \end{aligned} \quad (41)$$

Putting all arguments together,  $\forall \eta \in (0, 1)$ ,

$$\begin{aligned} \varrho(\eta_*) &= \max \left\{ \max\{h_{b_n}^{1/2}(\eta_*) \mid n \in \mathcal{N} \setminus \{N\}\}, (1 - \eta_*) \right\} \\ &\stackrel{(41)}{=} \max \left\{ h_{b_{N-1}}^{1/2}(\eta_*), (1 - \eta_*) \right\} \stackrel{(40)}{=} h_{b_{N-1}}^{1/2}(\eta_*) \\ &\leq h_{b_{N-1}}^{1/2}(\eta) \leq \max \left\{ h_{b_{N-1}}^{1/2}(\eta), (1 - \eta) \right\} \\ &\stackrel{(41)}{=} \max \left\{ \max\{h_{b_n}^{1/2}(\eta) \mid n \in \mathcal{N} \setminus \{N\}\}, (1 - \eta) \right\} \\ &= \varrho(\eta), \end{aligned}$$

where the first inequality holds because of Lemma 9 and  $b_{N-1} \in (0, 1/2)$ . The previous result establishes Theorem 6.

## REFERENCES

- [1] D. Bertsekas and J. N. Tsitsiklis, *Neuro-Dynamic Programming*. Athena Scientific, 1996.
- [2] D. Bertsekas, *Reinforcement Learning and Optimal Control*. Athena Scientific, 2019. [Online]. Available: <https://books.google.co.jp/books?id=ZiBlyQEACAAJ>
- [3] R. S. Sutton and A. G. Barto, *Reinforcement Learning: An Introduction*. Cambridge, MA: MIT Press, 2018.
- [4] D. Ormonet and S. Sen, "Kernel-based reinforcement learning," *Machine Learning*, vol. 49, pp. 161–178, 2002.

- [5] M. G. Lagoudakis and R. Parr, "Least-squares policy iteration," *J. Mach. Learn. Res.*, vol. 4, pp. 1107–1149, Dec. 2003.
- [6] A. Nedić and D. P. Bertsekas, "Least squares policy evaluation algorithms with linear function approximation," *Discrete Event Dynamic Systems*, vol. 13, no. 1, pp. 79–110, Jan 2003. [Online]. Available: <https://doi.org/10.1023/A:1022192903948>
- [7] D. P. Bertsekas, V. S. Borkar, and A. Nedić, "Improved temporal difference methods with linear function approximation," *Learning and Approximate Dynamic Programming*, pp. 231–255, 2004.
- [8] X. Xu, D. Hu, and X. Lu, "Kernel-based least squares policy iteration for reinforcement learning," *IEEE Transactions on Neural Networks*, vol. 18, no. 4, pp. 973–992, 2007.
- [9] J. Bae, P. Chhatbar, J. T. Francis, J. C. Sanchez, and J. C. Principe, "Reinforcement learning via kernel temporal difference," in *IEEE EMBS*, 2011, pp. 5662–5665.
- [10] W. Sun and J. A. Bagnell, "Online Bellman residual and temporal difference algorithms with predictive error guarantees," in *International Joint Conference on Artificial Intelligence*, 2016, pp. 4213–4217.
- [11] A.-M. Farahmand, M. Ghavamzadeh, C. Szepesvári, and S. Mannor, "Regularized policy iteration with nonparametric function spaces," *J. Machine Learning Research*, vol. 17, no. 1, pp. 4809–4874, 2016.
- [12] Y. Akiyama, M. Vu, and K. Slavakis, "Nonparametric Bellman mappings for reinforcement learning: Application to robust adaptive filtering," *IEEE Transactions on Signal Processing*, vol. 72, pp. 5644–5658, 2024.
- [13] A. H. Sayed, "Adaptation, learning, and optimization over networks," *Foundations and Trends in Machine Learning*, vol. 7, no. 4-5, pp. 311–801, 2014.
- [14] D. Bertsekas, "Distributed dynamic programming," *IEEE Transactions on Automatic Control*, vol. 27, no. 3, pp. 610–616, 1982.
- [15] K. Cai and G. Chen, "A distributed path planning algorithm via reinforcement learning," in *China Automation Congress (CAC)*, 2022, pp. 3365–3370.
- [16] A. Mathkar and V. S. Borkar, "Distributed reinforcement learning via Gossip," *IEEE Transactions on Automatic Control*, vol. 62, no. 3, pp. 1465–1470, 2017.
- [17] P. Pennesi and I. C. Paschalidis, "A distributed actor-critic algorithm and applications to mobile sensor network coordination problems," *IEEE Transactions on Automatic Control*, vol. 55, no. 2, pp. 492–497, 2010.
- [18] S. Valcarcel Macua, J. Chen, S. Zazo, and A. H. Sayed, "Distributed policy evaluation under multiple behavior strategies," *IEEE Transactions on Automatic Control*, vol. 60, no. 5, pp. 1260–1274, 2015.
- [19] S. Kar, J. M. F. Moura, and H. V. Poor, "QD-learning: A collaborative distributed strategy for multi-agent reinforcement learning through consensus + innovations," *IEEE Transactions on Signal Processing*, vol. 61, no. 7, pp. 1848–1862, 2013.
- [20] V. Mnih, A. P. Badia, M. Mirza, A. Graves, T. Lillicrap, T. Harley, D. Silver, and K. Kavukcuoglu, "Asynchronous methods for deep reinforcement learning," in *International Conference on Machine Learning*, ser. Proceedings of Machine Learning Research, M. F. Balcan and K. Q. Weinberger, Eds., vol. 48. New York, New York, USA: PMLR, 20–22 Jun 2016, pp. 1928–1937. [Online]. Available: <https://proceedings.mlr.press/v48/mnih16.html>
- [21] J. Foerster, I. A. Assael, N. De Freitas, and S. Whiteson, "Learning to communicate with deep multi-agent reinforcement learning," *Advances in Neural Information Processing Systems*, vol. 29, 2016.
- [22] D. Lee, H. Yoon, and N. Hovakimyan, "Primal-dual algorithm for distributed reinforcement learning: Distributed GTD," in *Conference on Decision and Control (CDC)*. IEEE, 2018, pp. 1967–1972.
- [23] X. Zhao, P. Yi, and L. Li, "Distributed policy evaluation via inexact ADMM in multi-agent reinforcement learning," *Control Theory and Technology*, vol. 18, pp. 362–378, 2020.
- [24] K. Zhang, Z. Yang, H. Liu, T. Zhang, and T. Başar, "Finite-sample analysis for decentralized batch multiagent reinforcement learning with networked agents," *IEEE Transactions on Automatic Control*, vol. 66, no. 12, pp. 5925–5940, 2021.
- [25] P. Bianchi and J. Jakubowicz, "Convergence of a multi-agent projected stochastic gradient algorithm for non-convex optimization," *IEEE Transactions on Automatic Control*, vol. 58, no. 2, pp. 391–405, 2013.
- [26] N. Aronszajn, "Theory of reproducing kernels," *Transactions of the American Mathematical Society*, vol. 68, pp. 337–404, 1950.
- [27] B. Schölkopf and A. J. Smola, *Learning with Kernels: Support Vector Machines, Regularization, Optimization, and Beyond*, ser. Adaptive Computation and Machine Learning. MIT Press, 2002. [Online]. Available: <https://books.google.co.jp/books?id=y8ORL3DWt4sC>
- [28] L. Györfi, M. Kohler, A. Krzyżak, and H. Walk, *A Distribution-Free Theory of Nonparametric Regression*. New York: Springer, 2010.
- [29] A. Rahimi and B. Recht, "Random features for large-scale kernel machines," in *NIPS*, vol. 20, 2007.
- [30] J. L. Gross, J. Yellen, and M. Anderson, *Graph Theory and Its Applications*, 3rd ed. CRC Press, 2019.
- [31] S. Boyd, N. Parikh, E. Chu, B. Peleato, and J. Eckstein, *Distributed Optimization and Statistical Learning via the Alternating Direction Method of Multipliers*, ser. Foundations and Trends in Machine Learning. Now Publishers, 2011.
- [32] K. Slavakis and I. Yamada, "Fejér-monotone hybrid steepest descent method for affinely constrained and composite convex minimization tasks," *Optimization*, vol. 67, no. 11, pp. 1963–2001, 2018.
- [33] R. B. Bapat, *Graphs and Matrices*, 2nd ed., ser. Texts and Readings in Mathematics. Hindustan Book Agency, 2011, no. 58.
- [34] A. Ben-Israel and T. N. E. Greville, *Generalized Inverses: Theory and Applications*, 2nd ed., ser. CMS Books in Mathematics. Springer, 2003.
- [35] E. Kreyszig, *Introductory Functional Analysis with Applications*, ser. Wiley Classics Library. Wiley, 1991.
- [36] H. H. Bauschke and P. L. Combettes, *Convex Analysis and Monotone Operator Theory in Hilbert Spaces*. New York: Springer, 2011.
- [37] J. Nocedal and S. J. Wright, *Numerical Optimization*, 2nd ed., ser. Springer Series in Operations Research and Financial Engineering. Springer, 2006.
- [38] T. M. Apostol, *Mathematical Analysis*, 2nd ed., ser. Addison-Wesley Series in Mathematics. Addison Wesley, 1974.
- [39] M. Towers, A. Kwiatkowski, J. Terry, J. U. Balis, G. De Cola, T. Deleu, M. Goulão, A. Kallinteris, M. Krimmel, A. KG, R. Perez-Vicente, A. Pierré, S. Schulhoff, J. J. Tai, H. Tan, and O. G. Younis, "Gymnasium: A standard interface for reinforcement learning environments," 2024. [Online]. Available: <https://arxiv.org/abs/2407.17032>
- [40] Inverted pendulum. [Online]. Available: [https://gymnasium.farama.org/environments/classic\\_control/pendulum/](https://gymnasium.farama.org/environments/classic_control/pendulum/)
- [41] M. Shil and G. N. Pillai, "Inverted pendulum control using twin delayed deep deterministic policy gradient with a novel reward function," in *IEEE Delhi Section Conference (DELCON)*, 2022, pp. 1–6.
- [42] Cartpole. [Online]. Available: [https://gymnasium.farama.org/environments/classic\\_control/cart\\_pole/](https://gymnasium.farama.org/environments/classic_control/cart_pole/)